

## MASTER

### Design, fabrication and testing of a point-of-care microfluidic chip integration of on-chip blood separation and luminescence detection

Moonen, E.J.M.

*Award date:*  
2019

[Link to publication](#)

#### **Disclaimer**

This document contains a student thesis (bachelor's or master's), as authored by a student at Eindhoven University of Technology. Student theses are made available in the TU/e repository upon obtaining the required degree. The grade received is not published on the document as presented in the repository. The required complexity or quality of research of student theses may vary by program, and the required minimum study period may vary in duration.

#### **General rights**

Copyright and moral rights for the publications made accessible in the public portal are retained by the authors and/or other copyright owners and it is a condition of accessing publications that users recognise and abide by the legal requirements associated with these rights.

- Users may download and print one copy of any publication from the public portal for the purpose of private study or research.
- You may not further distribute the material or use it for any profit-making activity or commercial gain

# **Design, fabrication and testing of a point-of-care microfluidic chip**

*Integration of on-chip blood separation and luminescence  
detection.*

E.J.M. Moonen  
0895596

Supervisor:

Prof. dr. ir. J.M.J. den Toonder

Committee:

Prof. dr. M. Merkx  
dr. H. Wyss  
ir. E.A. van Aalen

Department of Mechanical Engineering  
Microsystems

Eindhoven, October 2019



# Abstract

Analyte detection from body fluids is of fundamental importance in making medical decisions and optimising personalised medicine. Current detection in centralised laboratories tends to be expensive, laborious and can take valuable time. Therefore, many research is done into point-of-care testing (POCT). POCT is defined as medical diagnostic testing near the patient and increases the speed, costs and ease of testing. This research shows the use of the LUMABS sensor assay in a microfluidic POCT chip, developed in the group of Prof. M. Merckx at the TUE, to detect antibodies from whole blood. This LUMABS sensor is based on bioluminescence resonance energy transfer (BRET) and starts emitting light upon addition of the NanoGlo substrate. This emitted light shows a transition from green to blue when the LUMABS sensor makes contact with a specific antibody. The POCT consists of a microfluidic chip with a passive on-chip plasma extraction structure and two chambers. In these chambers the LUMABS sensor and the NanoGlo substrate are pipetted. After addition of the test sample the chip fills passively and starts emitting light. The colour of the emitted light can be detected with a DSLR camera in a dedicated measurement set-up. The images taken can be analysed using a Matlab script to obtain the green/blue-ratio from were the antibody concentration can be deducted.



# Contents

<b>Contents</b>	<b>v</b>
<b>1 Introduction</b>	<b>1</b>
1.1 LUMABS . . . . .	2
1.2 Aim and outline of project . . . . .	2
<b>2 Background</b>	<b>5</b>
2.1 Point-of-care testing . . . . .	5
2.1.1 Requirements for POCT devices . . . . .	5
2.1.2 Microfluidic POCT . . . . .	5
2.2 LUMABS . . . . .	8
2.3 Blood separation . . . . .	10
<b>3 Methods</b>	<b>17</b>
3.1 Device design . . . . .	17
3.2 Device fabrication . . . . .	17
3.2.1 Hydrophilic channels . . . . .	18
3.3 Assay addition . . . . .	19
3.4 Blood separation . . . . .	20
3.5 Luminescence detection . . . . .	21
3.6 Image analysis . . . . .	22
3.7 Experiments . . . . .	23
<b>4 Results and discussion</b>	<b>25</b>
4.1 Plasma extraction . . . . .	25
4.2 Capillary filling of the device . . . . .	26
4.3 Antibody detection . . . . .	27
4.3.1 Stabilisation of the ratio . . . . .	27

4.3.2	Device calibration . . . . .	28
4.3.3	Intensity . . . . .	29
4.3.4	Effects of Pluronic F-127 . . . . .	30
4.4	Detection in blood plasma . . . . .	31
5	Conclusions and outlook	33
	Bibliography	35
	Appendix	39
A	Milling details	39
B	Pluronic F-127 durability	40
C	Inkjet printing	41
D	Blood collection by fingerprick	42
E	Plasma extraction	45
F	Appendix Matlab	49
G	Diffusion in the chip	54
H	TU/e code of scientific conduct	55

# Chapter 1

## Introduction

Point-of-care testing (POCT), also called bedside testing, is defined as medical diagnostic testing at or near the patient. This point-of-care testing eliminates the need for complex laboratory set-ups and reduces the time between sample taking and diagnosis. Currently, the range of POCT includes devices for the qualitative and/or quantitative determination of a range of analytes from body fluids, like blood, urine, saliva and sweat. The analytes that can be determined include glucose, cardiac markers, alcohol, drugs, infectious pathogens and nucleic acids. Microfluidic lab-on-a-chip technologies are considered as promising technologies that can meet one of the most important requirements of a POCT device, since it can miniaturise and integrate most of the methods used in standard laboratories into a small chip. POCT enables fast medical decisions, since the diseases can be diagnosed at a very early stage. For many diseases a quick detection and treatment increases the health outcomes for patients. Furthermore, POCT can enable better monitoring of treatment by regularly measuring the concentrations of a specific drug in a patient. One of the many examples where POCT can be used is for therapeutic drug monitoring (TDM) of cancer treatment. Unfortunately, the successful treatment of cancer is usually not possible without damage to healthy tissue and organs. Research shows that the risk of noncancer deaths, partly caused by treatment, now surpasses that of cancer deaths, particularly for young patients in the year after diagnosis [1]. Side effects and noncancer deaths caused by treatment could be reduced by giving patients exactly the right amount of treatment. Besides the three common treatment approaches: surgery, chemotherapy and radiotherapy, immunotherapy has been investigated worldwide as the fourth treatment approach. Immunotherapy is a relatively new type of cancer treatment that uses the immune system of the patient to fight the cancer. Immunotherapy may work by stopping or slowing down the growth of cancer cells, by helping the immune system to recognise and destroy cancer cells or by reducing the chance of metastasis. Immunotherapy holds the potential to becoming more precise and personalised, with potentially fewer side effects.

The number of POCT devices used in the market has steadily increased over the decades since its introduction [2]. However, research conducted under primary care doctors in Australia, Belgium, the Netherlands, the UK and the USA showed a desire for more POCT devices to help them diagnose a broader range of acute and chronic conditions [3]. Therefore, a lot of research is currently being conducted, both at the start of the process developing novel methods as well as in the final steps taking the products to the market.



## 1.1 LUMABS

In the Biomedical Engineering department at Eindhoven University of Technology in the group of Professor Maarten Merkx a sensor assay is developed that allows detection of antibodies from blood [4]. Currently, the sensor is developed for antibodies against HIV1-p17, hemagglutinin (HA), dengue virus type I and for the therapeutic antibodies Her2-receptor targeting trastuzumab, the anti-CD20 antibodies rituximab and obinutuzumab, the anti-TNF-alpha adalimumab and the EGFR-blocking cetuximab [5]. The antibodies trastuzumab, rituximab, obinutuzumab and cetuximab are used for immunotherapy against cancer. These novel sensors, called LUMABS, are based on bioluminescence resonance energy transfer (BRET) and will show a colour shift in the emission when in contact with the antibodies. After the development of the sensor complex, it was clear that this detection mechanism would be ideal for application in POCT devices. Therefore, the Microsystems group of Professor Jaap den Toonder in the Mechanical Engineering department at Eindhoven University of Technology started a research into the development of a POCT device for the detection of antibodies in blood using the LUMABS sensor complex.

## 1.2 Aim and outline of project

This research aims to design, fabricate and validate a microfluidic point-of-care test using the LUMABS assay as detection method. In this specific project the LUMABS sensor CTX-LUMABS-2 will be used for testing the detection of the therapeutic antibody cetuximab from whole blood. This master graduation project is part of the Printing makes sense project. This project aims to use printing techniques, like 3D printing and inkjet printing to develop a POCT device for analyte detection from blood using the LUMABS assay. Previous work done by master students showed the feasibility of the use of the LUMABS assay in a microfluidic chip. However, inconsistent results did not yet show a quantitative proof for the detection of cetuximab in a POC test. Furthermore, the designed microfluidic chip was not yet suitable for usage with whole blood. Figure 1.1 shows a schematic overview of the steps that need to be taken in order to incorporate the LUMABS assay in a POCT device. As with any POCT device, the first step is to apply the sample to the system. In this case the working liquid is blood, and separation of the blood is necessary since the auto-fluorescence of red blood cells can give substantial background noise in the luminescence measurement [6]. The next step in the LUMABS POCT device is the addition of the sensing assay, which consist of the substrate Nano-Glo and the LUMABS sensor as is described in more detail in section 2.2. In between steps capillary forces will transport the liquid through the system. The final step in the POCT device is the read-out of the result.

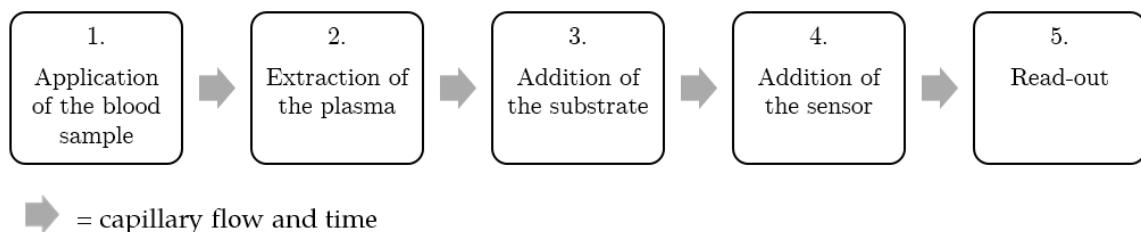


Figure 1.1: Schematic overview of the necessary steps to take to use the LUMABS assay in a POCT device from application of the sample to read-out.

The first goal of this graduation project is the integration of passive on-chip plasma extraction from whole blood. The second goal of this project is the addition of the LUMABS assay in the microfluidic chip. This goal consists of three parts, the first being the physical application of the assay, this can be done by pipetting or inkjet printing. The second is the determination of the amount of sensor and substrate needed in such a small volume microfluidic chip. The amount or concentration of sensor added depends on the affinity of the sensor to the antibody in the microfluidic chip. The concentration needs to be high enough to detect the antibodies and give enough luminescence but needs to be low enough to be able to detect low concentrations of antibody. Thirdly, the preservation of sensor and substrate in the chip needs to be studied. Finally, the detection of the emitted light and calibration of the POCT chip are studied. Furthermore, multiple changes are made in the chip design to ensure optimal flow through the system.

Chapter 2 will give background information on POCT devices, the LUMABS assay and blood separation. Chapter 3 will describe the methods used during the project, including device fabrication, blood separation, luminescence detection and image analysis. Chapter 4 will describe and discuss the results obtained during the project. Finally, conclusions are drawn and recommendations towards a POCT device ready for clinical usage are given in Chapter 5.



# Chapter 2

## Background

### 2.1 Point-of-care testing

#### 2.1.1 Requirements for POCT devices

Besides being suitable to operate at the bedside, at home or at the doctors office, a POCT device needs to meet more requirements. A complete POCT device should strive to meet the following requirements:

- The device should be sensitive enough to be used with a small volume, usually around one droplet (max. 100  $\mu\text{L}$ ) of fluid taken from the patient.
- The duration of the total procedure from taking the sample to obtaining results should be minimal, desirably within minutes.
- The device must be simple to use by a person with minimal medical training or even by the patient him- or herself.
- The consumables involved in the process must be robust for storage and usage. The storage of the consumables should have no influence on the result of the test.
- The obtained results should be according to the established laboratory method.
- The number of parts and steps to obtain a result should be minimal. Therefore, no or limited sample preparation should be necessary.

#### 2.1.2 Microfluidic POCT

Using microfluidic technologies a wide spectrum of POCT devices can be developed. From a range of body fluids a lot of analytes can be determined using a clever combination of microfluidic processes and detection techniques. Figure 2.1 shows an overview of possibilities within the field of microfluidic POCT.

##### *Analyte*

When defining a new POCT technique, the first thing to determine is which analyte should be detected. The different analytes include proteins [7], cells [8], nucleic acids [9], viruses [10], bacteria [11] and metabolites [12].

### *Fluid*

For detection of an analyte, body fluid from a patient is taken and used as input for the microfluidic system. These body fluid include blood [13], saliva [14], sweat [15], urine [16], tears [17] and exhaled breath [18].

### *Microfluidic chip - processes*

Within the microfluidic chip all processes that are usually executed in a centralised laboratory need to be integrated. The first thing that could be necessary when a fluid sample is put in the chip is obtaining the correct volume or concentration of analyte necessary for detection. Processes that are further used for this are sampling, dilution, amplification, filtering, separation and/or extraction. Next, usually a sensor or reactant needs to be combined and mixed with the sample. Depending on the complexity of the POCT device these processes run in parallel or series and could involve multiple cycles of steps [19, 20, 21, 22].

### *Microfluidic chip - fluid manipulation*

Usually a POCT microfluidic chips needs a mechanism to transport the fluid through the chip. This transport can happen passively or actively. The most favourable transport mechanism for a POCT device would be a passive mechanism as this requires no external additions to the microfluidic chip. Currently, the passive mechanism most used for transport in microfluidic chips is by hydrophilic capillary forces [22]. These forces are generated due to the design of the microfluidic channels. Furthermore, paper-based devices also use the capillary force which is generated in the paper [23]. Besides the passive mechanisms, also active mechanism can be used to transport the fluid through the POCT chip. These external forces could be mechanical [24], magnetic [25], thermal [26] or electrical [26].

### *Microfluidic chip - material*

The choice of materials for the POCT microfluidic chip depends on various factors such as the desired function, optical properties, physiochemical properties, fabrication techniques and the potential applications. Possible materials for POCT microfluidic chips could be inorganic materials, like silicon [27], glass [28] and ceramics [29], polymers [30] or paper [31].

### *Detection*

One of the key components in any POCT device is the detection mechanism. In the field of POCT a broad range of detection methods is available. The possible range of techniques include optical, electrical, electrochemical, magnetic and dimension measurements, as well as spectroscopy, electrophoresis and calorimetric techniques [9].

### *Results*

The final step in any POCT device is the read-out of results. A quantitative result in concentration would give the most precise result. However, in some cases a qualitative result already gives all the necessary information.

Overview POCT devices based on microfluidic technologies

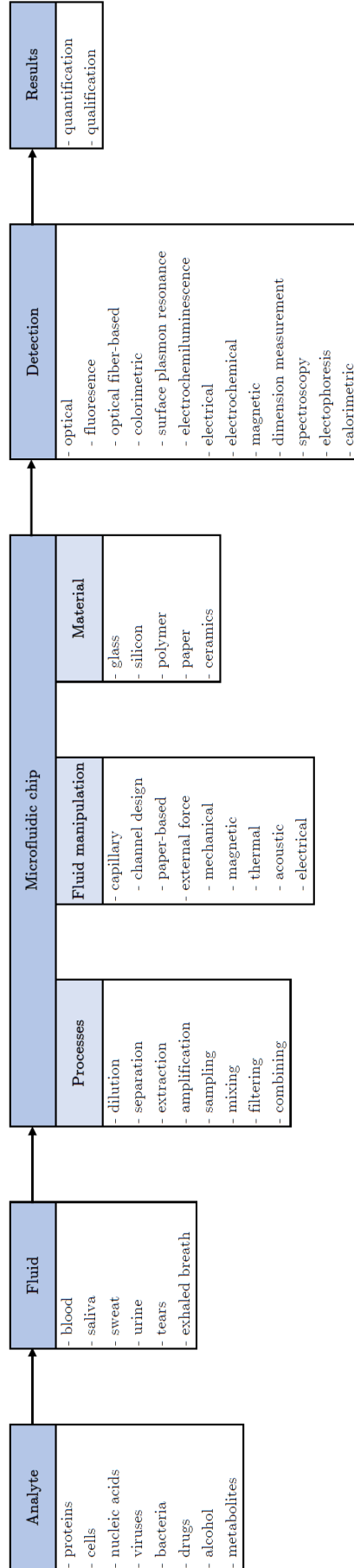


Figure 2.1: Overview of microfluidic POCT. References are found in the main text.

## 2.2 LUMABS

One of the most important components in any POCT device is the detection mechanism. In the Biomedical Engineering department at Eindhoven University of Technology in the group of Professor Maarten Merckx a sensor platform has been developed that allows detection of antibodies directly in solution [4]. This sensor format, called LUMABS, is based on bioluminescence resonance energy transfer (BRET) between the luminescent enzyme NanoLuc and fluorescent protein mNeonGreen. NanoLuc emits blue light upon addition of its substrate and is connected via a semiflexible linker to mNeonGreen, which is green fluorescent. This reaction happens in the presence of the substrate furimazine, when the substrate is acted upon by the reaction, light is given off as a by-product. The linker keeps both proteins together and contains two identical epitopes which facilitates binding to a specific antibody, schematically shown in Figure 2.2. In the absence of the specific antibody, the proximity of the two proteins will result in efficient BRET and emission of green light. Binding of an antibody to the epitope, will result in the disruption of the interaction between the helper domains, increased distance between the BRET-pair, and consequently in the emission of green light. The concentration of target antibody can be determined by the ratio between the blue and green emissions ( $g/b$ -ratio).

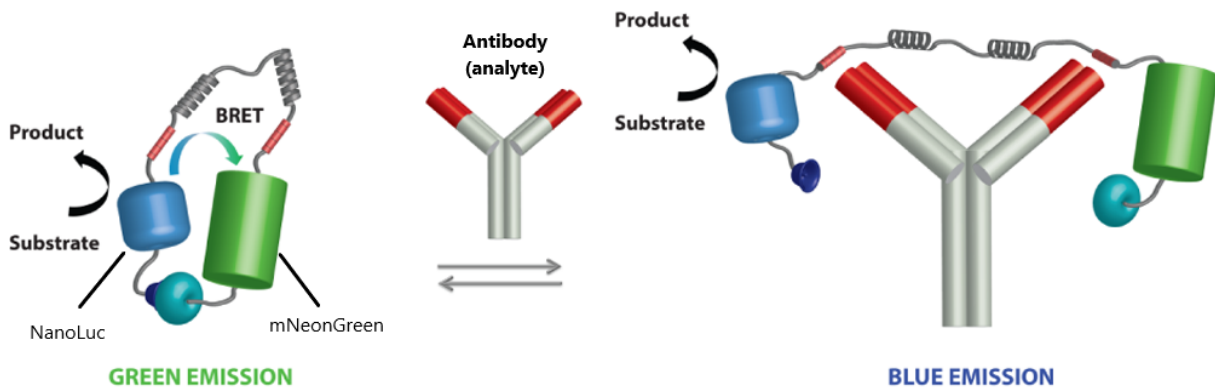


Figure 2.2: Schematic representation of LUMABS sensor concept. The luciferase NanoLuc and the acceptor protein mNeonGreen are held in close proximity by two helper domains, which leads to efficient BRET. Bivalent binding of an antibody to the epitopes in the semi-flexible linker between mNeonGreen and NanoLuc separates the BRET partners apart, shifting the emission from green-blue to blue. Image adapted from [4].

The CTX-LUMABS-2, designed for the detection of cetuximab, is used in this project. Figure 2.3A shows the luminescence emission spectra of this sensor, in which two clear emission peaks are visible, one for mNeonGreen at 517 nm which is slightly higher than the NanoLuc peak at 460 nm, suggesting a closed sensor state. Upon addition of 1.5  $\mu\text{M}$  cetuximab, the sensor is opened and the emission peak of mNeonGreen decreases, resulting in a lower  $g/b$ -ratio. Figure 2.3B can be derived from Figure 2.3A when multiple experiments with different concentrations of cetuximab are done. Figure 2.3B shows the normalised green to blue emission ratio for antibody titrations to 100 pM of sensor. A typical s-shaped curve is visible with the detection range around the clinical concentrations of therapeutic antibodies used for immunotherapy in blood.

The NanoLuc is significantly brighter than other typically used luciferases, which is beneficial for detection since it requires less sensitive equipment [32]. Furthermore, the modular architecture of the LUMABS sensor allows for variation in epitope sequence, increasing the amount of potential targets. Currently, sensors have been developed to measure/detect antibodies against HIV1-p17, hemagglutinin (HA), dengue virus type I and the therapeutic antibodies Her2-receptor targeting trastuzumab, the anti-CD20 antibodies rituximab and obinutuzumab, the anti-TNF-alpha adalimumab

and the EGFR-blocking cetuximab [5]. Therefore, the LUMABS sensor complex is ideal for application in multiplexed POCT devices. Currently, the LUMABS assay is used in a wells plate and measurements take place in a plate reader, the step towards POCT devices is not yet realised.

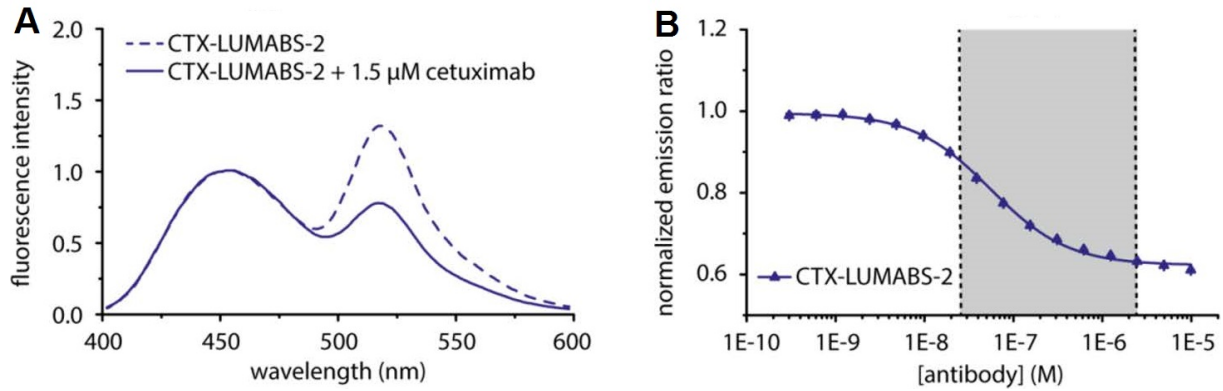


Figure 2.3: Characterisation of the CTX-LUMABS-2 assay for the detection of cetuximab. (A) Luminescence emission spectra of 100 pM with or without the indicated amount of the target antibody and normalised at 460 nm. (B) The normalised green to blue emission ratio for antibody titrations to 100 pM of sensor. Data represent mean from triplicate measurements. Image adapted from [5]



## 2.3 Blood separation

Currently, the developed POCT chip works with a model solution of PBS in which the analytes are dissolved. However, for real applications the POCT device needs to work with whole blood. Therefore, on-chip separation of blood cells from the plasma needs to be integrated. In the plasma various biomarkers are present, including proteins, metabolites and circulating nucleic acids. Figure 2.4 shows an overview of the composition of blood [33]. For this project it is necessary to separate the plasma from the blood cells in order to detect the antibodies that are contained within the plasma. An antibody, also known as an immunoglobulin, is a large, Y-shaped protein that is used by the immune system to neutralise pathogens such as pathogenic bacteria and viruses. The size of an antibody is about 10 nm, which is small compared to a red blood cell (6-8  $\mu\text{m}$ ), white blood cell (5-17  $\mu\text{m}$ ) or platelets (2-3  $\mu\text{m}$ ) [34]. Therefore, this size difference is commonly exploited in separation techniques.

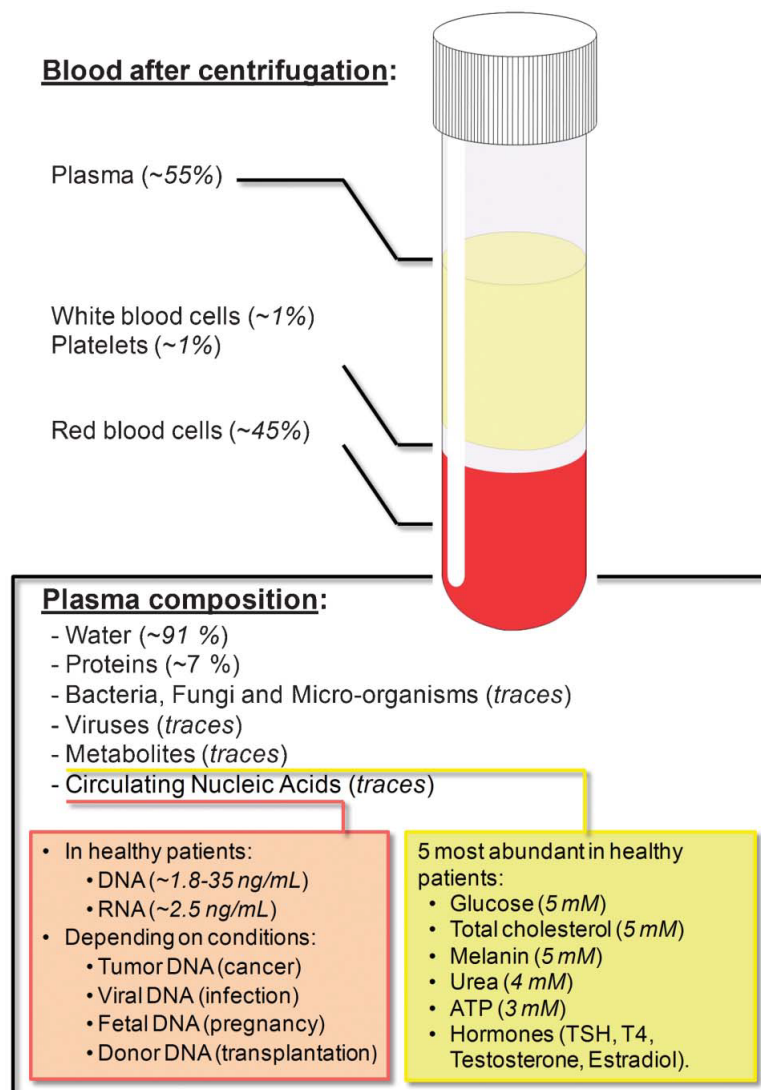


Figure 2.4: Composition of blood [33].

Current state-of-art laboratory equipment for the separation of blood would be a centrifuge or a filtering device. These batch processes have variable waiting times, include multiple handling steps and require relatively big machines. Therefore, research is being conducted into the development of micro-scale blood separation techniques. As can be seen in Figure 2.5 the developed techniques can be divided into three main technique categories, namely microfluidic chip-based, centrifuge-based and paper-based. In the category of microfluidic chip blood separation, techniques can be found that are either passive or active. Passive blood separation techniques rely on physical forces within the blood flow to induce plasma extraction from the blood cells. These techniques can be either membrane-based, density-based or geometry-based. Active separation techniques need external forces for the separation, these forces could be either mechanical which makes the technique flow-based or these forces could be induced by an external field, which can be either acoustic, electric or magnetic.

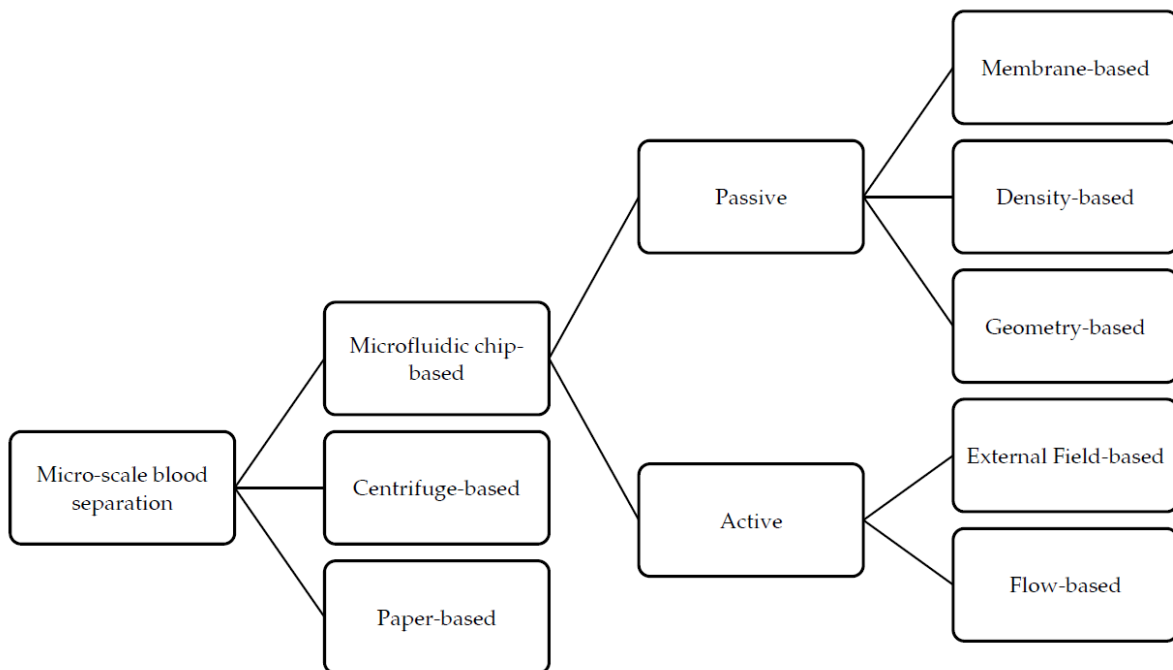


Figure 2.5: Micro-scale separation techniques for the separation of whole blood into blood cells and plasma.

### Microfluidic-based - Passive

A passive technique relies on separation without external force needed. The blood needs to flow through the system using capillary forces and pumping equipment should not be necessary. Practically speaking, this technique would be most suited for POCT applications since it requires no external equipment and thus reduces the complexity of the device. The first category of passive techniques is the membrane-based separation technique. This technique relies on a membrane, also called filter, which is incorporated into the microfluidic channel. As in its macroscale counterpart, microfiltration is based on the size difference of the different components in the blood. Several different filtering membranes are available with differences in pore size, capacity and filtering efficiency [35]. Membrane-based filtration is one of the most commonly used blood separation techniques in microfluidic chips, Figure 2.6 shows some examples of membrane-based blood separation chips. A selection has been made from multiple papers, but techniques that require washing of the membrane or pumping of the blood are eliminated since they do not classify as completely passive. However, as is also the case with the chip shown in 2.6C, dilution of the sample is sometimes still necessary. As can be seen from the examples, the performance of the microfluidic chips differs a lot, from 36  $\mu\text{L}$  to 4  $\mu\text{L}$  of plasma extracted from whole blood. Furthermore, the time necessary to extract the plasma also varies strongly between different papers from half a minute up to 20 minutes.

A different membrane-based technique that is used in microfluidic chips to separate plasma from whole blood, is the use of beads as filter structure [36]. Closed packed beads are in these chips used as membrane. However, preliminary dilution of the blood or active retraction of the plasma from the system is usually necessary.

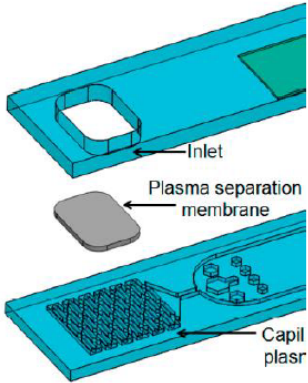
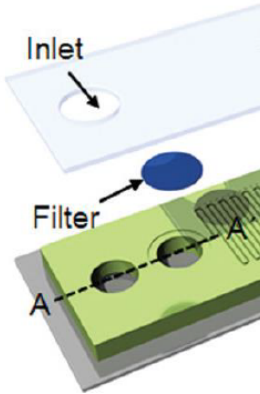
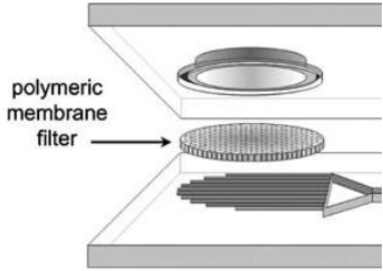
Membrane-based separation		
Membrane with capillary pump [34]	Gravity-assisted filter-in-top design [35]	Membrane with hydrophilic PDMS [36]
<p><b>A</b></p> 	<p><b>B</b></p> 	<p><b>C</b></p> 
Commercial Vivid separation membrane	Pore size: 0.4 $\mu\text{m}$	Pore size: gradient 30-5 $\mu\text{m}$ and 0.40-0.45 $\mu\text{m}$
Plasma separation: 36 $\mu\text{L}$ from 45 $\mu\text{L}$ of whole blood	Plasma separation: up to 4 $\mu\text{L}$	Dilution to 10-30% v/v
No leakage	Slow process and yield	RBC leakage or hemolysis

Figure 2.6: Membrane-based blood separation techniques from literature. (A) Membrane-based filtration technique using an off-the-shelf membrane and capillary pump for optimised separation. Image adapted from [37]. (B) Gravity-assisted filter-in-top design for blood separation. Optimised system, but slow process and yield. Image adapted from [38]. (C) Membrane-based blood separation using polydimethylsiloxane (PDMS). Preliminary dilution of blood to 10-30% v/v is necessary. Image adapted from [39].

The next category of passive microfluidic chip-based blood separation techniques is density-based separation, also called gravity-assisted separation or sedimentation. Sedimentation is one of the oldest techniques used for separation of blood. Microfluidic chips that are based on sedimentation for blood separation simply rely on weight differences and thus gravitational differences of the different components of whole blood. Sedimentation velocity of red blood cells ranges from  $0.27$  to  $3.8 \mu\text{m s}^{-1}$ , depending on the health and sex of the patient [40]. In literature some examples can be found of density-based microfluidic blood separation techniques. In Figure 2.7 two of these techniques are shown. The technique in Figure 2.7A relies on sedimentation in a short distance over a trench, this results in an efficient separation of the heavier blood cells to the bottom of the trench [41]. When the system is kept in a low pressure environment before usage, the plasma is sucked out to the chamber at the top. The example in Figure 2.7B relies on time for blood cells to separate and sink to the bottom of the channel [42]. Unfortunately, the paper does not describe the process in depth. Due to the fact that the system only relies on time, the separation time is as long as 8 minutes. The plasma yield of this technique is reasonable at  $6 \mu\text{L}$  of plasma from  $27 \mu\text{L}$  of whole blood. However, the paper does not mention the purity of the obtained plasma, which can be important for detection of antibodies.

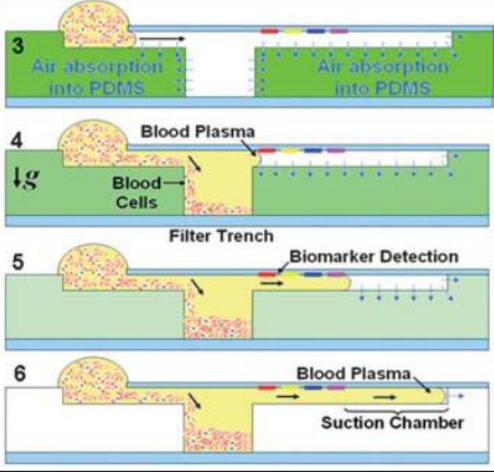

Density-based separation	
Sedimentation in trench [38]	Time dependent sedimentation [39]
<p><b>A</b></p> 	<p><b>B</b></p>  <p><b>Deposition of blood and sedimentation chamber</b></p>
100% purity of the obtained plasma	$6 \mu\text{L}$ of plasma from $27 \mu\text{L}$ of whole blood
Device activation in a low-pressure necessary to induce enough capillary force	8 minutes necessary for the separation

Figure 2.7: Density-based blood separation techniques from literature. (A) Density-based separation technique using sedimentation in a trench. 100% purity of the plasma can be reached in this microfluidic chip. Image adapted from [41]. (B) Density-based separation technique using time dependent sedimentation. Separation needs time and yield is not very high.  $6 \mu\text{L}$  of plasma can be extracted from  $27 \mu\text{L}$  of whole blood. Image adapted from [42].

The last category of passive microfluidic chip-based blood separation techniques is geometry-based separation. In this technique, the natural or forced deviation of the different components during flow of the blood through or along specific geometrical features is exploited to extract plasma from whole blood. Figure 2.8 shows two examples in which the geometry of the microfluidic channel is used to separate the plasma from the blood. The example in Figure 2.8A uses a 3D fishbone structure to extract the plasma from the whole blood. The depth of the fishbone structure is only  $2\ \mu\text{m}$  and therefore blood cells stay in the straight channel that has a depth of  $100\ \mu\text{m}$  and are collected in the blood cell reservoir. The plasma is deviated into the fishbone structure and directed to the plasma reservoir. This technique yields  $1.5\ \mu\text{L}$  highly pure plasma from  $10\ \mu\text{L}$  whole blood after 75 seconds. The example in Figure 2.8B uses diamond shaped obstacles to extract plasma from whole blood. The plasma yield in this technique is lower and the time required is higher. However, the plasma has a high purity for this technique as well.

Geometry-based separation	
Separation using fishbone structure	Separation by obstacles
<p><b>A</b></p>	<p><b>B</b></p>
10 $\mu\text{L}$ whole blood separated in 75 s	5 $\mu\text{L}$ whole blood separated in 3 to 5 minutes
1.5 $\mu\text{L}$ plasma from 10 $\mu\text{L}$ blood	0.1 $\mu\text{L}$ plasma from 5 $\mu\text{L}$ blood
<99.9 % plasma purity	98% plasma purity

Figure 2.8: Geometry-based blood separation techniques from literature. (A) Geometry-based separation technique using a fishing bone structure to deviate the cells from the plasma. This technique has a high plasma yield with high purity within a short amount of time. Image adapted from [43]. (B) Geometry-based separation technique using diamond shaped obstacles to separate the plasma from the blood cells. Image adapted from [44].

### Microfluidic-based - Active

An active blood separation technique relies on the application of external force in order to separate the plasma from the blood cells. When a mechanical force is applied due to flow the separation can be classified as flow-based. All other active techniques can be classified as external-field-based. These external fields can be acoustic, electrical, or magnetic.

Figure 2.9 shows three examples of blood separation techniques based on the application of external fields. Figure 2.9A shows an example of a separation technique based on the application of acoustic waves to whole blood [45]. The acoustic waves induce agglomeration of blood cells in the middle of the channel. Although the technique works and can separate good quality plasma, the technique is not yet fully integrated into a microfluidic chip format. Furthermore, pumps are required to pump the blood through the channels. Figure 2.9B shows an example of the combination of using a magnet and a filter

to extract plasma from whole blood [46]. In this technique two magnets are used and moved to induce force that squeezes the plasma through the filter. This technique yields a large amount of high purity plasma in one minute and can be integrated in microfluidic POCT chips. Figure 2.9C shows an example of blood separation using dielectrophoresis [47]. Dielectrophoresis is a phenomenon in which a force is exerted on a dielectric particle when it is subjected to a non-uniform electric field. This force does not require the particle to be charged. The strength of the force on different particles, cells in this case, depends strongly on the particles electrical properties, shape and size. This device is able to separate 165 nL of plasma from a 15  $\mu\text{L}$  sample in 15 minutes and is fully integrated into a microfluidic chip format.

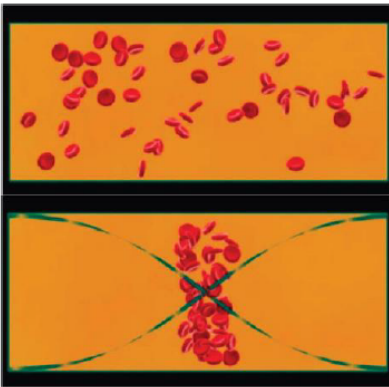
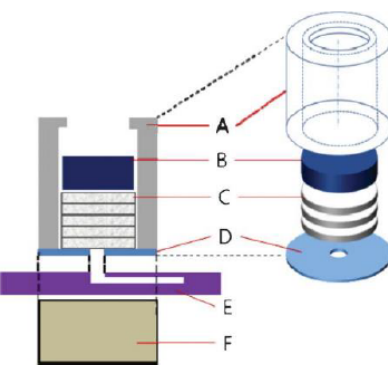
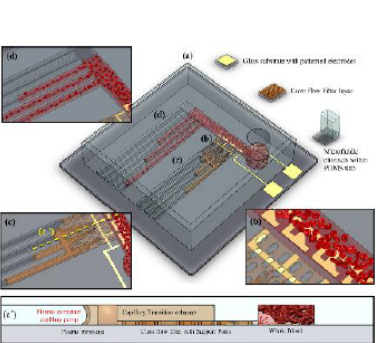
External-Field-based separation		
Separation using acoustic waves	Magnetically actuated separation combined with filter	Separation using dielectrophoresis
<b>A</b> 	<b>B</b> 	<b>C</b> 
Pumping necessary	Purity: 99.999%	180 nL cell-free plasma
Good quality plasma	Plasma recovery: 30%	165 nL plasma from 15 $\mu\text{L}$ of whole blood
Not yet fully developed for integration in POCT chip	Operation time; 1 min	15 $\mu\text{L}$ separated in 15 minutes

Figure 2.9: External-Field-based blood separation techniques from literature. (A) Blood separation using acoustic waves. Image adapted from [45]. (B) Blood separation using a magnetic field created by two magnets (B and F) combined with a filter (C). Image adapted from [46]. (C) Blood separation using dielectrophoresis. Image adapted from [47]

Another category of active microfluidic blood separation techniques is the category of flow-based techniques. The external force in this case is the mechanical force that is used to induce flow through the system. This category can be seen as an additional category to a lot of techniques, since most commonly flow only is not enough to separate blood. Therefore, every technique that is part of a different category that requires an induced flow through the system can also be classified as a flow-based system. However, for POCT application flow-based separation techniques are not desired since it requires additional machines and steps, which makes the process more complicated.

### Centrifuge-based

At macro-scale a centrifuge is a commonly used machine for the separation of blood. Therefore, research has been done into miniaturising this technique for usage with smaller volumes of blood and thus smaller machines. One major technique that has been developed is the CD-format for blood separation [48]. This technique utilises a process similar in movement to a CD in a CD-player. Figure 2.10 shows the channel lay-out of the separation channel as proposed in [48]. This channel lay-out lies 32 mm from the

centre of rotation on a disk that has a diameter of 120 mm. This centrifuge-based technology can extract  $2 \mu\text{L}$  plasma from  $5 \mu\text{L}$  of whole blood at a spinning frequency of 40 Hz within 20 seconds. The residual cell concentration in the plasma is less than 0.11%. While this can classify as a blood separation at micro-scale it is not completely suited for uses in POCT application. However, when on-chip separation is not possible this could be an easy technique to use in clinical POCT applications as the device necessary is still smaller than conventional laboratory equipment.

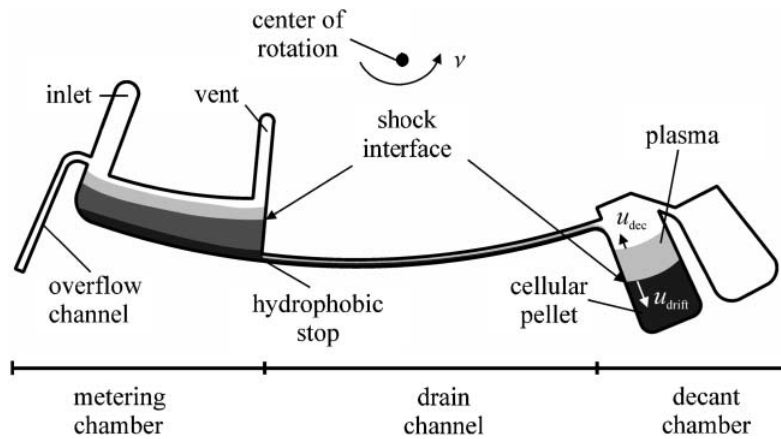


Figure 2.10: Flow scheme of the 'CD-format' blood separation technique using centrifugal forces. A metered volume of the blood sample defined between hydrophobic stop and overflow channel flows from the metering chamber via the drain channel into the decant chamber. A shock interface separating plasma from the whole blood builds out in all parts of the network and proceeds radially outwards. When enough plasma is extracted it flows into the plasma collection chamber. The blood cells are being forced outwards due to the circular rotation of the disk [48].

### Paper-based

The last category in the overview of micro-scale blood separation techniques is the paper-based technique. In POCT applications paper has been widely used for lateral-flow assays such as glucose and pregnancy tests. But more recently, paper devices are also being developed for the separation of plasma from blood. In this case paper-based devices belong in a separate category as they differ from membrane-based devices with a paper filter, since these devices are entirely made out of paper. These all-paper devices are called microfluidic paper-based analytical devices ( $\mu\text{PADs}$ ). One example of such a device is shown in Figure 2.11 [49]. This device separates plasma from a finger-prick volume of whole blood and uses this plasma for identification of antibodies in a colorimetric assay.

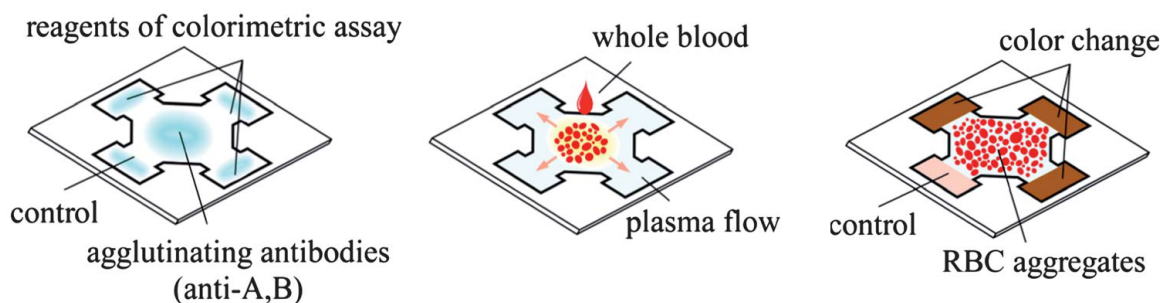


Figure 2.11: Design of a microfluidic paper-based device ( $\mu\text{PAD}$ ) with integrated blood separation. Image adapted from [49].

# Chapter 3

## Methods

### 3.1 Device design

After an extensive literature study choices were made for the design of the POCT test. First, choices were made for the design of the plasma extraction mechanism. As can be seen in Figure 2.5 some choices had to be made. In the category of microfluidic chip-based extraction method a division is made in passive and active techniques. As explained in section 2.1.1 one of the requirements for a POCT device is that it must be simple to use and that the number of steps towards a result should be minimal. Therefore, it was chosen to design a passive plasma extraction technique. In the category of passive techniques, three main categories were identified: membrane-, density- and geometry-based plasma extraction techniques. Multiple examples from literature were studied, which led to the choice for a membrane-based plasma extraction technique. This choice was mainly made because this technique is commonly used in literature. Furthermore, geometry-based techniques required the design and fabrication of a far more complicated structure. In density-based techniques usually PDMS was used for the fabrication, which is not an ideal material for mass production or 3D printing.

The next design consideration was the lay-out of the other parts of the chip. As can be seen in Section 2.2, the LUMABS assay consists of two reagents, the substrate and the LUMABS sensor. Therefore, it was chosen to use two chambers which are connected by channels. To accommodate drying of the reagents in the chambers, the chambers were made slightly deeper than the channels.

### 3.2 Device fabrication

Figures 3.1 and 3.2 respectively show an overview of the parts of the POCT chip and an assembled chip. The chip consists of five parts: the microfluidic structure (1), the sealing film (2), the plasma extraction membrane (3), a layer of double sided tape (4) and a well (5).

The bottom part of the POCT chip is the capillary microfluidic structure. This capillary structure is made from 0.3 mm thick polymethyl methacrylate (PMMA) and is machined with a Roland MDX-40A micromilling machine, more details on this fabrication procedure can be found in Appendix A. Figure 3.3 shows a drawing with dimensions of the PMMA structure. The capillary structure consists of four sections that are connected with channels. From inlet to outlet, the four sections are: the capillary



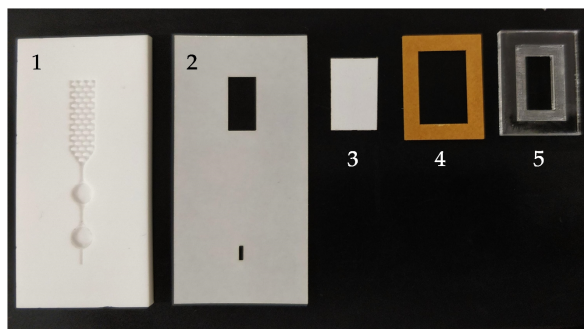


Figure 3.1: Overview of the different parts of the device. (1) PMMA capillary microfluidic structure (2) sealing film (3) plasma extraction membrane (4) double-sided tape (5) PMMA well.

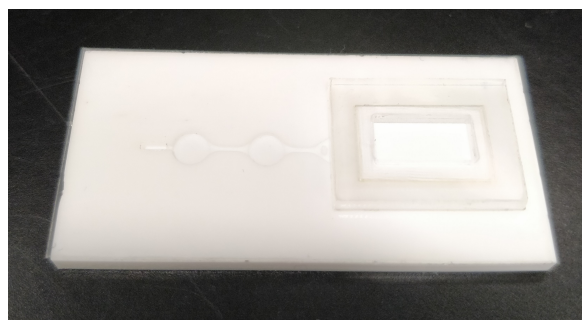


Figure 3.2: Assembled chip.

pump to facilitate plasma extraction, the substrate chamber, the detection chamber and the air outlet. The channels have a depth of 0.5 mm and the chambers of 0.7 mm. The design of the capillary pump and the plasma extraction membrane are explained in more detail in section 3.4. The substrate chamber and the detection chamber are both of the same size and each have a volume of  $8.8 \mu\text{L}$ . The total volume of the microfluidic structure is equal to  $48 \mu\text{L}$ .

The second part of the POCT chip is the sealing film. This film ensures a fluid tight sealing of the microfluidic structure. Currently, PCR wells plate sealing tape is used, which is cut to the correct size using a laser cutter from universal laser systems. The film has an inlet on which the plasma extraction membrane can be placed. Furthermore, the film has an outlet which is placed over the air outlet to ensure air can escape from the system during filling.

To ensure a safe and clean addition of the blood sample a well is placed on top of the inlet. The dimensions of the well can be found in Figure 3.4. The inner edge of the well is engraved with the laser cutter which gives a height difference of approximately 0.2 mm. By sticking the well to the PMMA chip with double sided tape the plasma extraction membrane is clamped in between the capillary structure and the well. This results in a fluid tight sealing which is essential for blood separation.

### 3.2.1 Hydrophilic channels

An important requirement of a functional POCT microfluidic chip is a completely passive fluid flow through the system. This passive fluid flow can be realised by using the capillary action. Capillary action is the ability of a liquid to flow in channels without the assistance of external forces, such as pumping. It occurs because of intermolecular forces between the liquid and surrounding solid surfaces, like the PMMA channel walls in the POCT chip. When these intermolecular forces increase in size, the capillary action increases. Therefore, it is important to facilitate an environment in which these intermolecular forces are maximised. One way to do this is by increasing the hydrophilicity of the channels.

In the designed POCT chip Pluronic F-127 is used to make the channels hydrophilic. Pluronic F-127 is a hydrophilic non-ionic surfactant, consisting of a central hydrophobic block of polypropylene glycol flanked by two hydrophilic blocks of polyethylene glycol (PEG). When this hydrophobic block can adhere to the hydrophobic PMMA surface, the hydrophilic blocks ensure a hydrophilic channel surface.

Pluronic F-127 was dissolved 2.5 w/v% in MilliQ water and the PMMA chips were submerged in this solution for 24 hours. This treatment reduced the contact angle from  $\sim 70^\circ$  to  $\sim 20^\circ$ . Preliminary durability tests showed a stability of the treatment after two weeks when kept in a vacuum sealing. The data of these tests can be found in Appendix B.

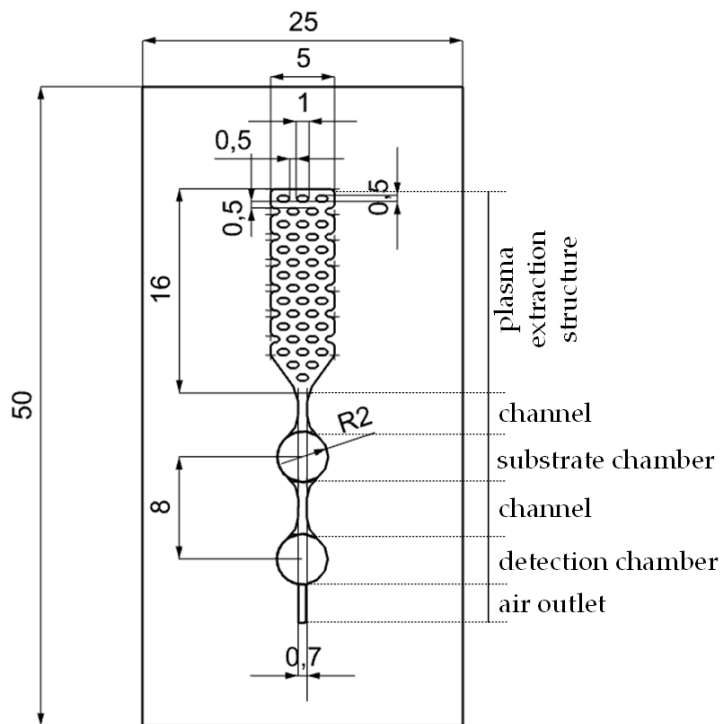


Figure 3.3: Dimensions in millimetres of the capillary structure on the PMMA chip. The chip is machined using a micromiller from a piece of 0.3 mm thick white PMMA. The channels have a depth of 0.5 mm and the chambers of 0.7 mm

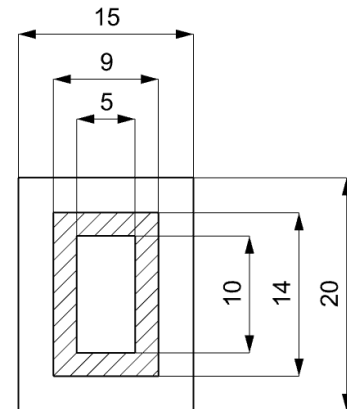


Figure 3.4: Dimensions of the well. The total thickness is equal to 2 mm, the hatched part has a thickness of 1.8 mm.

### 3.3 Assay addition

For this project the LUMABS sensor LUMABS-CTX-2 for the detection of cetuximab was used. After addition of the substrate this sensor emits green light, in the presence of the antibody cetuximab the colour of the light shifts to blue, as explained in Section 2.2.

The LUMABS reagents (sensor and substrate) were added in the POCT chip by pipetting. Before assembling the device, the substrate and LUMABS were added in the chambers and dried. One microlitre of ten times diluted stock solution substrate in PBS was added in the substrate chamber. The LUMABS was diluted to 200 nM in equal amounts of glycerol and PBS. One microlitre of this dilution was pipetted in the detection chamber, which leads to the addition of 200 fmol of LUMABS.

It was also explored to use inkjet printing to apply the LUMABS into the chamber. However, results were not promising and repeatable. More information on inkjet printing can be found in Appendix C.

### 3.4 Blood separation

The passive on-chip plasma extraction is facilitated by a structure consisting of two parts: a plasma extraction membrane and a capillary pumping structure. As plasma extraction membrane the commercially available Vivid plasma separation membranes grades GF and GR from Pall corporation were used [50]. These membranes are asymmetric with pores varying in size from large to small from top to bottom. This asymmetry allows the cellular components of the blood (red cells, white cells, and platelets) to be captured in the larger pores, while the plasma flows down into the smaller pores on the downstream side of the membrane. Enough capillary action is necessary in the channels under the filter membrane to wick the plasma from the membrane. Therefore, a capillary pump was designed which is situated under the filter membrane. The layout of the capillary pump structure including dimensions can be seen in Figure 3.5. This structure consists of pillars in channels which increase the surface area of the channel walls and thus increase the capillary action.

Whole human blood was purchased from Sanquin to test the plasma extraction. This blood was applied by pipetting in droplets of 50-100  $\mu\text{L}$  onto the filter membrane to study plasma extraction. Furthermore, a protocol for obtaining blood from finger pricks at the Microfablab was established. More information about this protocol can be found in Appendix D. More information about the design iterations towards to final design of the capillary pump can be found in Appendix E.

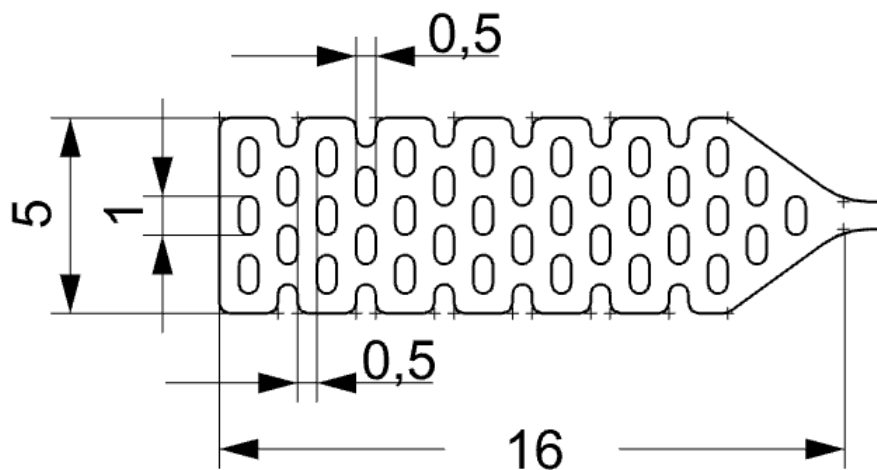


Figure 3.5: Close-up of the plasma extraction structure. Dimensions in millimetres.

### 3.5 Luminescence detection

After applying cetuximab dilution in PBS buffer with 0.5 mg/mL BSA on the inlet of the channel, the fluid will dissolve the substrate and LUMABS and will start emitting light. A Nikon D3300 DSLR camera was used for detection of the light. The Nikon D3300 is a camera with a 24.2 megapixel DX CMOS sensor and is equipped with a 18-55mm VR II kit lens. Images were taken with an exposure time of 30 seconds, ISO of 1600 and a f-number of 3.5. Furthermore, all automatic settings such as auto whitebalance were turned of.

A box was fabricated that blocks light from outside to allow for detection of the weak signal emitted from the POCT chip. The height of the box was determined by the minimal focal distance of the camera, when the height would be smaller, the POCT chip would not be in focus. Furthermore, the slot for the chip in the box ensures that the detection chamber is in the centre of the camera lens.

Every sample was measured over a period of 20 minutes, to obtain a g/b-ratio for the particular cetuximab concentration.



Figure 3.6: Luminescence detection set-up. Nikon D3300 digital slr camera on a black box containing the POCT chip. Dimensions hxwxd: 200x90x90 [mm].

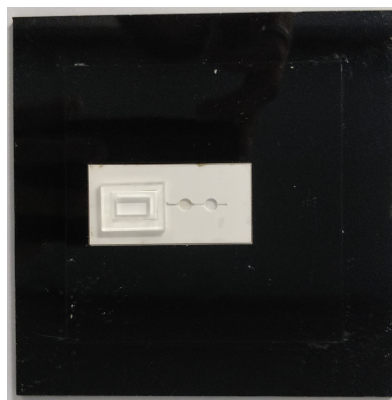


Figure 3.7: Chip in the slot in the camera box.

### 3.6 Image analysis

For analysis of the acquired photos, a Matlab script is written. This Matlab script enables a robust calculation of the green over blue ratio by eliminating variances in images. A schematic overview of the image analysis is shown in Figure 3.8. The complete code can be found in Appendix F.

The script starts by reading all photos and storing the RGB values into matrices. The next step is cropping of the images to only analyse the area of interest. Cropping is done semi-automatic, the user only needs to define the upper left corner of the detection chamber in the first image. The script then crops all images to the same rectangle. This manual step is necessary because in-between measurements the camera could have slightly moved. After cropping the script creates a greyscale image of the original image. The value of the greyscale of each pixel corresponds to the intensity of the luminescence. While analysing the data it was found that the intensity of luminescence in the image has an influence on the calculated g/b-ratio. Therefore, only pixels of one specific intensity are analysed. This is done by creating a binary image by comparing the values of the pixels in the greyscale image with a parameter called the luminescence threshold value. This threshold value is determined experimentally by choosing the highest luminescence value that at least 20 pixels have in each photo. After creating this binary image, the script finds the indices corresponding to the pixels equal to one. Next, using the acquired indices, the script saves the green and blue values of the corresponding pixels from the colour image. Finally, the green value of each pixel is divided by the blue value after which the mean g/b-ratio of one image is calculated. The final mean g/b-ratio is calculated by averaging the g/b-ratio of all chosen images. Furthermore, the Matlab script can also calculate the HSV values from which the hue value can be used in analysis.

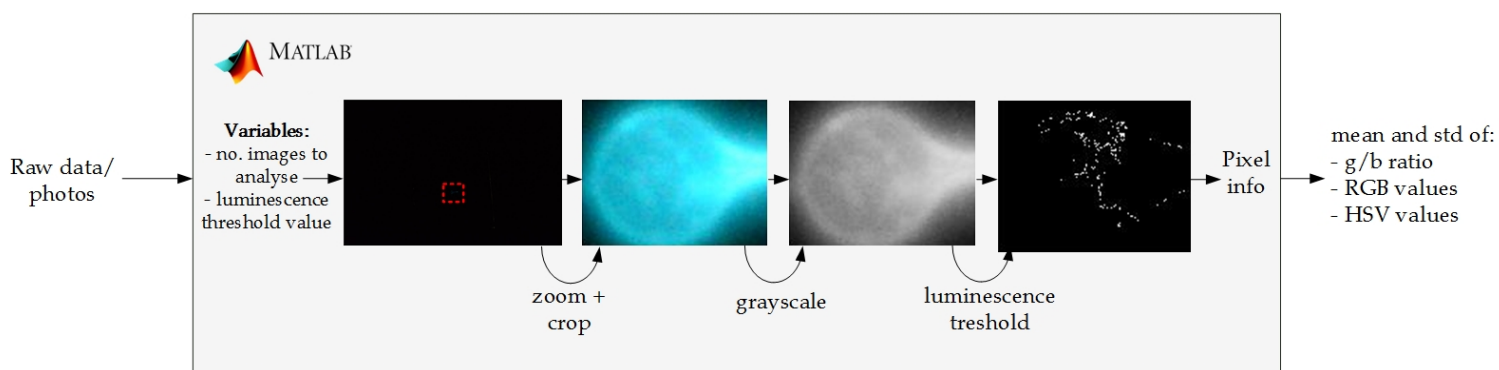


Figure 3.8: Schematic overview of the image analysis.

### 3.7 Experiments

For optimising, testing and characterising the POCT chip several experiments were done. The following table gives an overview of the executed experiments and their purpose.

Table 3.1: Important experiments performed during the project.

no.	Goal of the experiment	Chip	Medium	Cetuximab concentrations	Validation method
1	Validate the passive capillary action of the plasma extraction structure and test for leakage	Complete device	MilliQ water with food colour	-	Visual inspection
2	Test the plasma extraction	Plasma extraction structure only	Whole blood	-	Visual inspection
3	Check the operation of the available LUMABS	Chambers only transparent PMMA	PBS buffer	Ten-fold serial dilutions from 10000 nM to 1 nM	Plate reader
4	Test the POCT chip with the camera and determine a working amount of substrate and LUMABS	Chambers only transparent PMMA	PBS buffer	Ten-fold serial dilutions from 10000 nM to 1 nM	Camera
5	Make a calibration curve for the POCT device	Chambers only transparent PMMA	PBS/BSA buffer	Two-fold serial dilutions from 20000 nM to 0.3 nM	Camera
6	Make a calibration curve for the white POCT device	Chambers only white PMMA	PBS/BSA buffer	Two-fold serial dilutions from 20000 nM to 0.3 nM	Camera
7	Make a calibration curve for the POCT with blood plasma as working medium. Test the influence of the plasma extraction membrane on the detected cetuximab concentration	Complete device white PMMA	Pooled blood plasma	Two-fold serial dilutions from 20000 nM to 0.3 nM	Camera



## Chapter 4

# Results and discussion

### 4.1 Plasma extraction

The designed capillary structure is able to passively extract plasma from whole blood. Upon addition of the blood sample, the filter absorbs the droplet of blood. After waiting a few minutes the plasma starts flowing into the channel towards the substrate chamber. Figure 4.1 shows a transparent microfluidic chip from the bottom. It can be seen that the capillary pump is almost filled and soon the channel will start filling. It was observed that the capillary pump fills gradually row by row.

Although proof-of-concept is given, the time needed for filling the whole device is long and can be as long as 10-15 minutes. A possible cause for this lengthy filling time is that too little capillary action is created underneath the plasma extraction membrane. Enough capillary force is necessary to wick the plasma from the membrane into the channels. A possible way to increase the capillary action is by decreasing the size of the channels in the capillary pump. However, this means that a different fabrication technique (e.g. photolithography, soft lithography) needs to be used to create the microfluidic structure, since  $500\ \mu\text{m}$  is the smallest feature size that can be obtained with the micromilling technique. Furthermore, it was observed that the plasma extraction membrane absorbs quite a large volume of blood/plasma. This means that, when using plasma as working medium, up to  $100\ \mu\text{L}$  of plasma need to be placed on the membrane instead of the volume of the microfluidic structure of  $50\ \mu\text{L}$ .

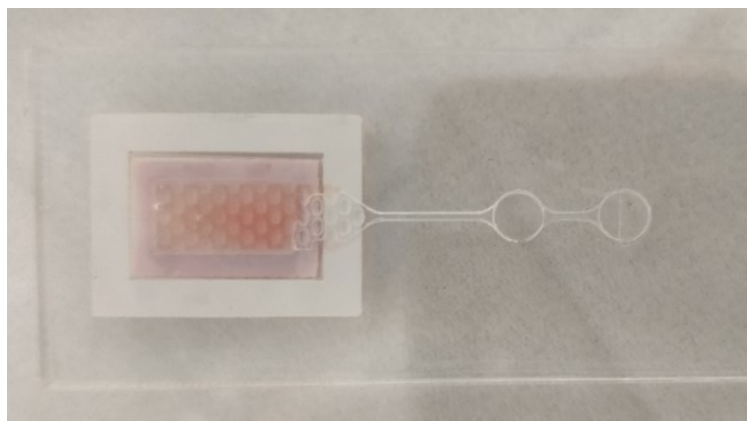


Figure 4.1: Bottom view of the transparent POCT chip. Plasma is being extracted underneath the membrane.



## 4.2 Capillary filling of the device

When using the hydrophilic Pluronic F-127 coating the capillary action in the device is enough to fill the channels and chambers completely. When using PBS/BSA buffer the system fills very quickly within several seconds. When using blood plasma as working fluid the system fill slightly slower in approximately 20 seconds. This difference in time is caused by the higher viscosity of plasma ( $\approx 1.5\text{-}1.7\text{mPa}\cdot\text{s}$ ) with respect to PBS/BSA buffer ( $\approx 1.05\text{ mPa}\cdot\text{s}$ ). This slower filling time can be beneficial since the substrate has more time to dissolve in the fluid before it enters the detection chamber.

Since the surface of the chip is hydrophilic, the substrate and LUMABS solution spread over the surface of the chambers upon addition. Due to capillary action more solution is attracted to the edges of the surface which leads to a non-uniform and non-repeatable spread of the assay components over the chambers. This effect can lead to an increased intensity at the edges of the chamber. However, this does not give inconsistencies in the analysed g/b-ratio. Sometimes the substrate and LUMABS spread not only over the chamber surface but also into the channels before drying. This leads to blocking of the channels which inhibits filling of the device. Therefore, before usage of the chip it needs to be inspected by eye to see whether the assay components blocks the channel.

During a part of the measurements, done in experiments 4 to 7 from Table 3.1, the LUMABS and substrate move through the device upon addition of the test sample. Figure 4.2 shows the movement over time. In these images the chamber on the left is the detection chamber. After capillary filling, luminescence is only seen from the detection chamber. After 20 minutes, the luminescence spreads over the full device. This is probably due to convection effects, since the timescale is too short for diffusion. In Appendix G an approximate diffusion calculation can be found.

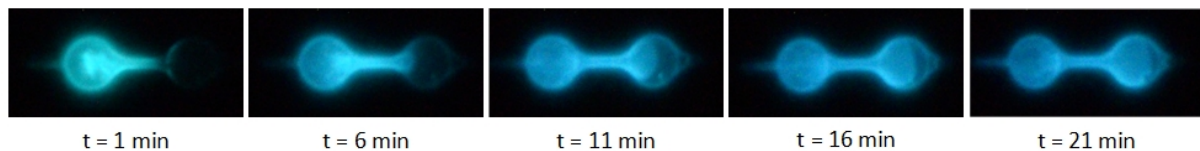


Figure 4.2: Diffusion of the LUMABS sensor and substrate in the device over time.

### 4.3 Antibody detection

The measurement results in this section are obtained in experiment 6 from Table 3.1. A microfluidic chip without the capillary pump structure and the plasma extraction membrane is used. This was done to reduce fabrication time and the use of the limited available plasma extraction membrane. Since the chambers and channels are the same in all experiments, the results will not be influenced. Additional tests were done to study the influence of the passage of the medium through the plasma extraction membrane. The results from these tests can be found in Section 4.4.

#### 4.3.1 Stabilisation of the ratio

The final measurements were executed over a time of 20 minutes, without incubation steps. Twenty minutes was chosen as the maximum duration, since this is the maximum time a POCT would desirably take. Furthermore, preliminary measurements of 60 minutes showed a stabilisation after 20 minutes. Figure 4.3 shows the  $g/b$ -ratio over time from 0 to 21 minutes. In the figure it can be seen that the ratio stabilises quickly in time. Furthermore, it can be seen that the stabilisation rate is higher in the presence of more antibody. However, the ratio stabilises fastest when little antibody is present since the difference in ratio at 0 minutes and the final ratio is smaller.

To minimise the variance caused by stabilisation of the result, the mean  $g/b$ -ratio over the images taken between 10 to 20 minutes is taken. It was also studied to take the mean over the images taken between 15-20 minutes or to only take the  $g/b$ -ratio of the last image, but this gave a larger standard deviation over multiple measurements.

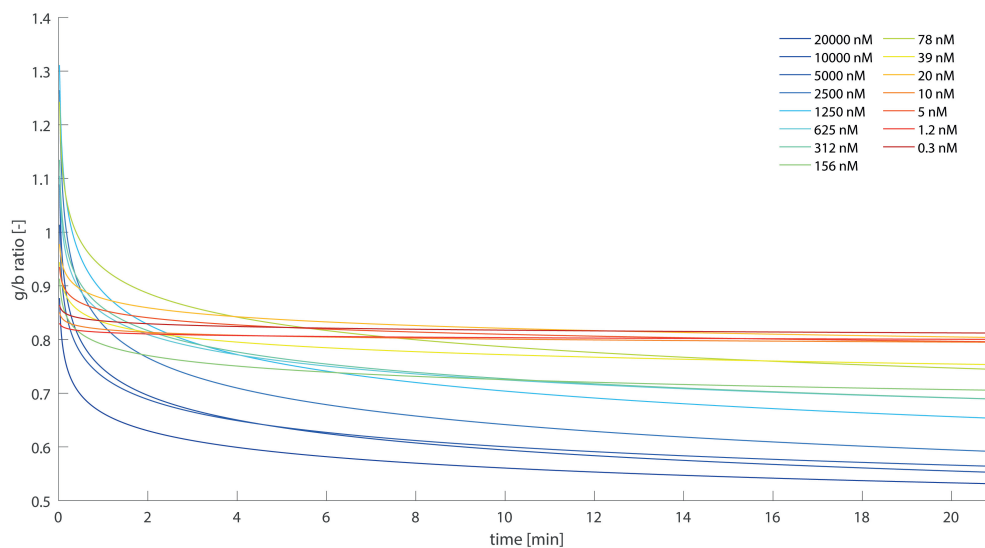


Figure 4.3:  $g/b$ -ratio versus time for different concentrations of cetuximab.

### 4.3.2 Device calibration

To make a calibration curve for the POCT chip a range of concentrations was measured over multiple days. The final calibration curve can be seen in Figure 4.4. The measurements for this curve were done in a white test chip for 20 minutes. The mean g/b-ratio over the last 10 photos (i.e. between 10 and 20 minutes) was taken as g/b-ratio for each particular cetuximab concentration. In total the measurements took six days, which led to a  $n = 4-6$  for each concentration. Everyday new cetuximab, LUMABS and substrate dilutions were made.

The curve fitted through the measurement data is given as [5]:

$$ER = \frac{(ER_{min} - ER_{max}) \times [Ab]}{(K_{d,app} + [Ab])} + ER_{max} \quad (4.1)$$

In this equation ER is the emission ratio at antibody concentration [Ab].  $ER_{min}$  is the emission ratio at sensor saturation and  $ER_{max}$  is the emission ratio in absence of antibody.  $K_{d,app}$  is the apparent dissociation constant. For this current calibration curve  $ER_{min}$  is equal to  $0.5565 \pm 0.018$ ,  $ER_{max}$  is equal to  $0.804 \pm 0.0125$  and  $K_{d,app}$  is equal to  $420 \text{ nM} \pm 157 \text{ nM}$ .

Dynamic range (DR) was calculated as the total change in emission ratio divided by the lowest ratio:

$$DR = \frac{ER_{max} - ER_{min}}{ER_{min}} = \frac{0.804 - 0.5565}{0.5565} = 0.4447 \quad (4.2)$$

The  $K_{d,app}$  is higher and the dynamic range (DR) is lower than the reported values in literature [5]. However, since the measurement environment is different, it can be expected that the fit parameters of the calibration curve are different.

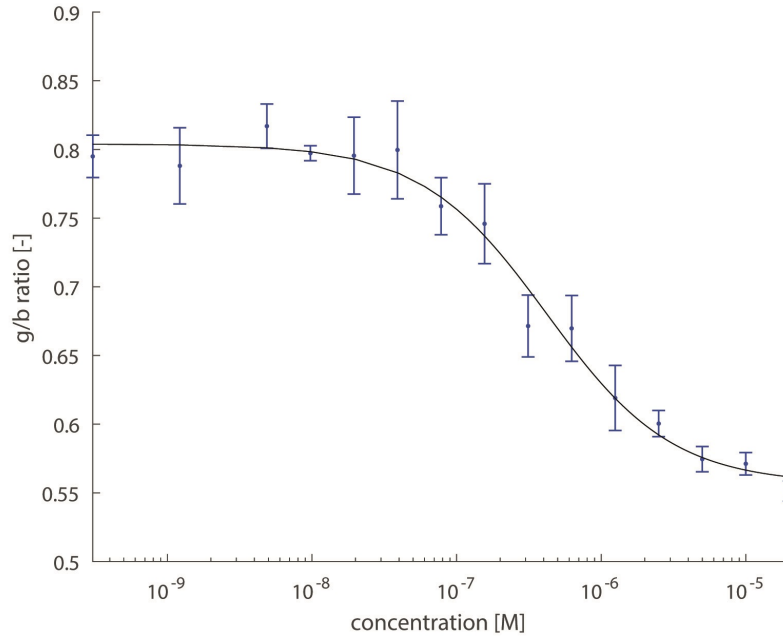


Figure 4.4: Calibration curve of the white POCT chip ( $n = 4-6$ ).

### 4.3.3 Intensity

Upon application of medium and filling of the device, the chip starts emitting light. Figure 4.5 shows the intensity in time for three different concentrations of antibody. It can be seen from the figure that the intensity stays almost constant in the 20 minutes. Some slight change can be seen in the homogeneity of the intensity due to diffusion of the assay components through the chamber. Since only pixels of a specific intensity are used for calculation of the g/b-ratio, as explained in Section 3.6, a slight change in intensity distribution or magnitude does not affect the results.

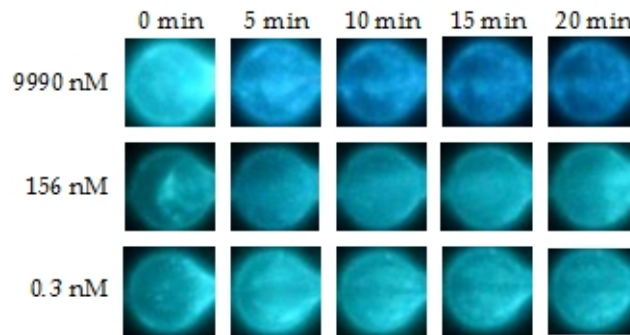


Figure 4.5: Change in intensity for different antibody concentrations. Measured in PBS buffer with 0.5 mg/mL BSA.

It was observed that the usage of white PMMA instead of transparent PMMA results in a slightly higher intensity. The white PMMA will reflect light and therefore the light output signal is maximised.

#### 4.3.4 Effects of Pluronic F-127

Pluronic F-127 is used to make the channels hydrophilic. However, it was observed that the usage of Pluronic F-127 has an effect on the LUMABS assay. Figure 4.6 shows the measured g/b-ratio versus time for different concentrations of cetuximab in PBS/BSA buffer. In this measurement Pluronic F-127 was diluted in MilliQ water at a concentration of 10 w/v%. When comparing Figure 4.6 with Figure 4.3 where the Pluronic F-127 did not had an effect, it can be seen that the results are different. As can be seen from Figure 4.6, the g/b-ratio decreases strongly and the mean g/b-ratios for different concentrations of cetuximab are incorrect. Instead of the trend seen in Figure 4.4, low concentrations of cetuximab now give a lower mean g/b-ratio than higher concentrations. This strong decrease in ratio can be caused by interference of the long Pluronic F-127 chains with the BRET of the LUMABS.

Experiments were done with different concentrations of Pluronic F-127 and it was found that when a dilution of 2.5 w/v% was used the Pluronic F-127 did not interfere with the LUMABS assay anymore.

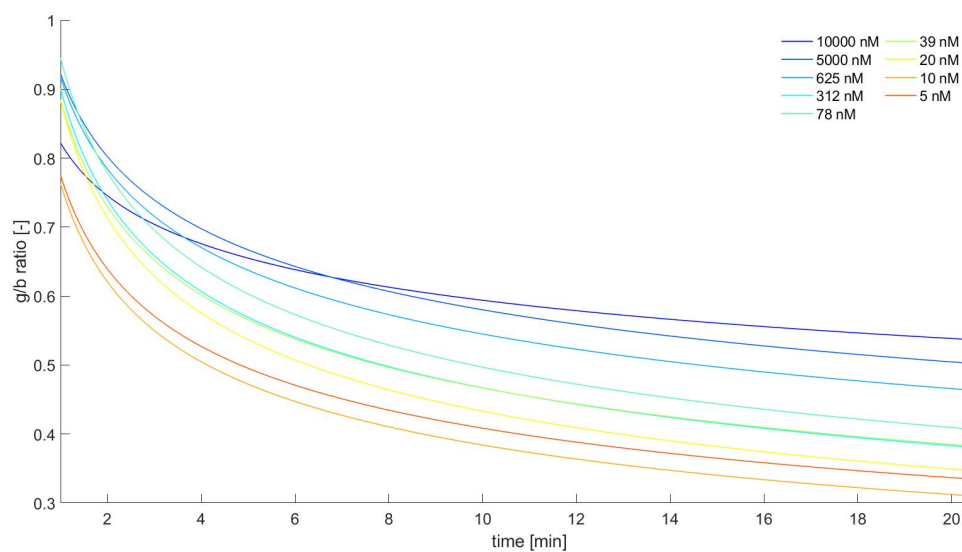


Figure 4.6: g/b-ratio versus time for different concentrations of cetuximab in PBS/BSA buffer. Pluronic F-127 (10 w/v% in MilliQ water) is used to increase the hydrophilicity of the PMMA chip.

## 4.4 Detection in blood plasma

As final experiment it was studied what the effects are of passing of the medium through the plasma extraction membrane. Furthermore, pooled blood plasma was used as working fluid in this experiment to approach the final application as closely as possible. The conditions are shown in Table 3.1, experiment number 7.

Figure 4.7 shows the  $g/b$ -ratio versus cetuximab concentration for the final POCT chip using pooled blood plasma as medium. Again Equation 4.2 is fitted through the data, yielding the following fit parameters:  $ER_{max} = 1.055 \pm 0029$ ,  $ER_{min} = 0.7144 \pm 0.0457$  and  $K_{d,app} = 541 \text{ nM} \pm 382 \text{ nM}$ . The dynamic range is equal to  $DR = 0.4775$ . Again, as in Section 4.3.2, the  $K_{d,app}$  is higher and the dynamic range (DR) is lower than the reported values in literature [5]. However, since the measurement environment is different, it can be expected that the fit parameters of the calibration curve are different.

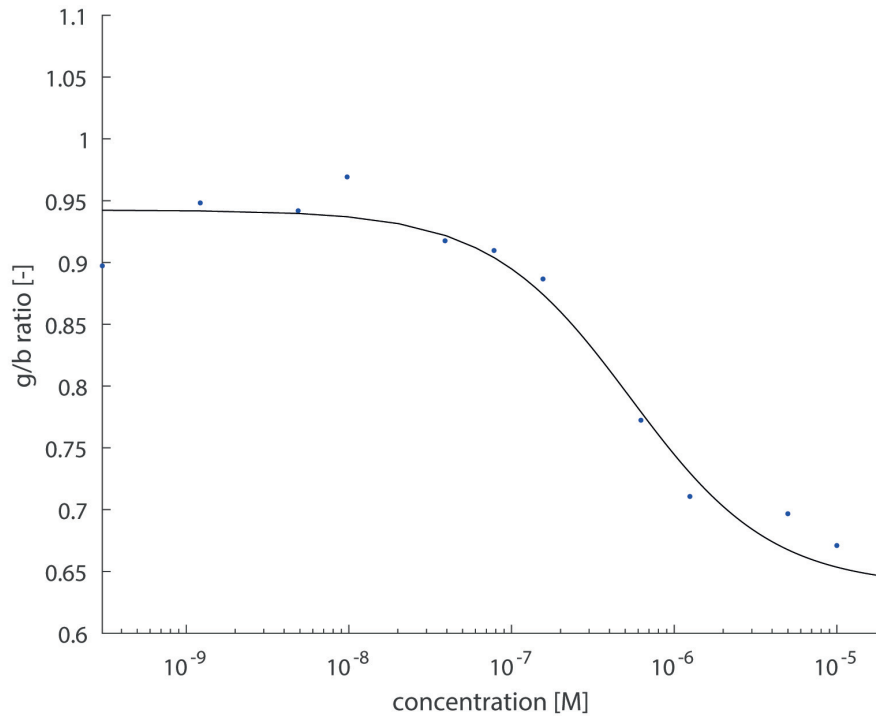


Figure 4.7: Calibration curve measured in the complete device including the filter with plasma as working fluid.

Figure 4.8 shows the calibration curve for the test chip with the PBS/BSA buffer as working medium (Fig. 4.4) and the calibration curve for the final chip with plasma as working medium (Fig. 4.7) to be able to compare the results directly. From the figure it can be seen that both curves have the expected s-shape. The curve from the plasma measurements is shifted towards higher  $g/b$ -ratios, this is an expected result from previous experiments done during the development of the LUMABS sensor and is mainly due to the fact that plasma absorbs more blue than green light [51]. Furthermore, the dynamic range for the measurements in the final chip with plasma appears to be slightly bigger with a difference of 0.0328. However, the curve of the plasma measurements is based on one data point for each cetuximab concentration. Therefore, no completely certain statement can be made.

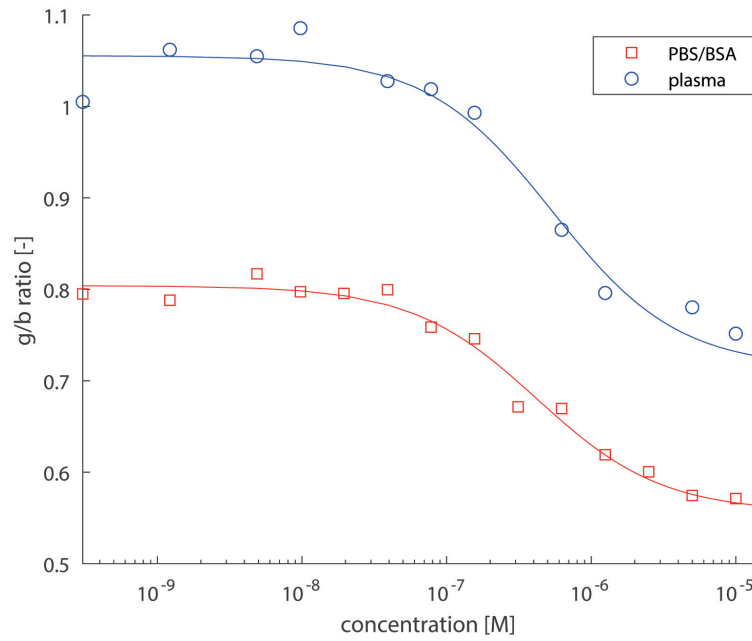


Figure 4.8: Comparison of the two calibration curves. The red line represents the calibration curve measured in the complete chip including the plasma extraction filter membrane with blood plasma as working medium ( $n = 1$ ). The black line represents the calibration curve in the test chip with PBS/BSA as working medium ( $n = 4-6$ ).

## Chapter 5

# Conclusions and outlook

A microfluidic point-of-care test has been developed for detection of the antibody cetuximab in buffer and blood plasma using the LUMABS assay. The POCT shows the applicability of the LUMABS assay in a microfluidic device and can be paired with a DSLR camera as method of detection. The chip is leak tight and after fabrication the chip functions passively upon application of the sample. Furthermore, a proof-of-concept capillary-driven plasma extraction structure has been developed. After improving the velocity of the plasma extraction, the developed POCT chip holds the potential to become a standardised test for antibody concentrations in blood.

The microfluidic structure is fabricated from PMMA using micromilling. To increase the capillary action, the hydrophilicity of the PMMA is increased by immersing the chip for 24 hours in a 2.5 w/v% Pluronic F-127 solution. The structure is sealed using a clear film to facilitate a fluid-tight chip. A laser cut PMMA well clamps the plasma extraction membrane on the microfluidic structure, finishing the POCT chip. Inside the chambers 1  $\mu\text{L}$  of 10 times diluted NanoGlo substrate and 200 fmol LUMABS protein in PBS/glycerol are added by pipetting and dried before sealing the chip. Upon addition of 100  $\mu\text{L}$  of fluid in the well, the chip fills by means of capillary action, the assay components dissolve and light is being emitted. After sealing the air outlet and placing the chip in a dark box, a DSLR camera is used to capture images. These images are analysed using a Matlab script to obtain the g/b-ratio. A calibration curve has been made for the usage of CTX-LUMABS-2 in the device. This curve shows the expected s-shape and the standard deviation including all variances looks promising. The Vivid GR/GF membranes from Pall corporation are used for on-chip passive plasma extraction. The membrane, in combination with a capillary pump, extracts plasma from whole blood which then passively flows into the channels and chambers.

In order to develop a standardised POCT that can be used in the clinic, two main topics need to be addressed next. The passive on-chip plasma extraction needs to be improved to decrease the time between sample taking and results, which is now around 30 minutes for cetuximab (10 minutes plasma extraction and 20 minutes detection). One way to do this is by increasing the capillary action created in the capillary pump underneath the plasma extraction membrane, which can be done by decreasing the cross-sectional size of the channels. Furthermore, a hydrophilic instead of hydrophobic sealing film should be used to increase the capillary action in the channels and chambers. The ARflow 93049 adhesive film from Adhesives Research can be used, since this is an optically clear film with a hydrophilic pressure-sensitive adhesive on one side.

The second topic that should be addressed is the detection set-up. Ideally a dedicated detection device is created that contains an optical sensor and gives the g/b-ratio on a small display after 20 minutes.



When these two topics are addressed a series of detection tests need to be done to establish the final standard deviation. When the final calibration curve including standard deviation is known, effects of changes to the microfluidic chip design (mixers, delays, etc.), usage of different materials, amount of sensor and substrate added and usage of hydrophilic coatings can be studied. Furthermore, inkjet printing of the LUMABS reagents in the chip, the preservation of the LUMABS in the chip and storage of the chip should be studied.

Ideally, the developed system works with different kinds of LUMABS sensors for the detection of other analytes in blood. It would be interesting to study what the results are of using different types of sensor in the same POCT chip. While not changing the detection set-up hardware and fabrication techniques, it should be tested whether the microfluidic chip is able to handle different LUMABS sensors. After testing small changes could be made to the design or detection if this is necessary.

Eventually, it would be great if an assortment of LUMABS POCT chips can be brought to the market to increase the ease of testing and improve patient care across diverse clinical settings.

# Bibliography

- [1] N G Zaorsky, T M Churilla, B L Egleston, S G Fisher, J A Ridge, E M Horwitz, J E Meyer, and Nicholas G Zaorsky. Causes of death among cancer patients. 1
- [2] Christopher P Price Andrew St John. Existing and Emerging Technologies for Point-of-Care Testing. 35(3):2–3, 2011. 1
- [3] Jeremy Howick, Jochen W.L. Cals, Caroline Jones, Christopher P. Price, Annette Plüddemann, Carl Heneghan, Marjolein Y. Berger, Frank Buntinx, John Hickner, Wilson Pace, Tony Badrick, Ann Van Den Bruel, Caroline Laurence, Henk C. Van Weert, Evie Van Severen, Adriana Parrella, and Matthew Thompson. Current and future use of point-of-care tests in primary care: An international survey in Australia, Belgium, The Netherlands, the UK and the USA. *BMJ Open*, 4(8), 2014. 1
- [4] Remco Arts, Ilona Den Hartog, Stefan E. Zijlema, Vito Thijssen, Stan H.E. Van Der Beelen, and Maarten Merckx. Detection of Antibodies in Blood Plasma Using Bioluminescent Sensor Proteins and a Smartphone. *Analytical Chemistry*, 88(8):4525–4532, 2016. 2, 8
- [5] Martijn van Rosmalen, Yan Ni, Daan F M Vervoort, Remco Arts, Susann K J Ludwig, and Maarten Merckx. Dual-Color Bioluminescent Sensor Proteins for Therapeutic Drug Monitoring of Antitumor Antibodies. *Analytical chemistry*, 90(5):3592–3599, 2018. 2, 9, 28, 31
- [6] Niteace C Whittington and Susan Wray. Suppression of Red Blood Cell Autofluorescence for Immunocytochemistry on Fixed Embryonic Mouse Tissue. *Current protocols in neuroscience*, 81:2.28.1–2.28.12, oct 2017. 2
- [7] Luc Gervais, Nico De Rooij, and Emmanuel Delamarche. Microfluidic chips for point-of-care immunodiagnosics. *Advanced Materials*, 23(24), 2011. 5
- [8] Hongying Zhu, Ikbal Sencan, Justin Wong, Stoyan Dimitrov, Derek Tseng, Keita Nagashima, and Aydogan Ozcan. Cost-effective and rapid blood analysis on a cell-phone. *Lab on a Chip*, 13(7):1282, mar 2013. 5
- [9] Lu Zhang, Baozhi Ding, Qinghua Chen, Qiang Feng, Ling Lin, and Jiashu Sun. Point-of-care-testing of nucleic acids by microfluidics. *TrAC - Trends in Analytical Chemistry*, 94:106–116, 2017. 5, 6
- [10] Cheng Cheng, Haochen Cui, Jayne Wu, and Shigetoshi Eda. A PCR-free point-of-care capacitive immunoassay for influenza A virus. *Microchimica Acta*, 184(6):1649–1657, jun 2017. 5
- [11] Nawfal Adam Mungroo, Gustavo Oliveira, and Suresh Neethirajan. SERS based point-of-care detection of food-borne pathogens. *Microchimica Acta*, 183(2):697–707, feb 2016. 5
- [12] Joseph Wang\*. Electrochemical Glucose Biosensors. 2007. 5
- [13] Frederic Bedin, Laurent Boulet, Elodie Voilin, Gerald Theillet, Agnes Rubens, and Christine Rozand. Paper-based point-of-care testing for cost-effective diagnosis of acute flavivirus infections. *Journal of Medical Virology*, 89(9):1520–1527, sep 2017. 6

- [14] Katrine Küllerich-Pedersen, Johannes Daprà, Solène Cherré, and Noemi Rozlosnik. High sensitivity point-of-care device for direct virus diagnostics. *Biosensors and Bioelectronics*, 49:374–379, nov 2013. 6
- [15] Aldo Roda, Massimo Guardigli, Donato Calabria, Maria Maddalena Calabretta, Luca Cevenini, and Elisa Michelini. A 3D-printed device for a smartphone-based chemiluminescence biosensor for lactate in oral fluid and sweat. 2014. 6
- [16] Chun-Che Lin, Chin-Chung Tseng, Tsung-Kai Chuang, Der-Seang Lee, and Gwo-Bin Lee. Urine analysis in microfluidic devices. 6
- [17] Ali K. Yetisen, Nan Jiang, Ali Tamayol, Guillermo U. Ruiz-Esparza, Yu Shrike Zhang, Sofía Medina-Pando, Aditi Gupta, James S. Wolffsohn, Haider Butt, Ali Khademhosseini, and Seok-Hyun Yun. Paper-based microfluidic system for tear electrolyte analysis. *Lab on a Chip*, 17(6):1137–1148, mar 2017. 6
- [18] Gaspard Pardon, Laila Ladhani, Niklas Sandström, Maxime Etori, Gleb Lobov, and Wouter van der Wijngaart. Aerosol sampling using an electrostatic precipitator integrated with a microfluidic interface. *Sensors and Actuators B: Chemical*, 212:344–352, jun 2015. 6
- [19] Michael Mauk, Changchun Liu, Jinzhao Song, Haim Bau, Michael G. Mauk, Changchun Liu, Jinzhao Song, and Haim H. Bau. Integrated Microfluidic Nucleic Acid Isolation, Isothermal Amplification, and Amplicon Quantification. *Microarrays*, 4(4):474–489, oct 2015. 6
- [20] Xiaoping Min, Da Fu, Jianzhong Zhang, Juntian Zeng, Zhenyu Weng, Wendi Chen, Shiyin Zhang, Dongxu Zhang, & Shengxiang Ge, Jun Zhang, and Ningshao Xia. An automated microfluidic chemiluminescence immunoassay platform for quantitative detection of biomarkers. 6
- [21] O Strohmeier, M Keller, F Schwemmer, S Zehnle, D Mark, F Von Stetten, R Zengerle, and N Paust. Centrifugal microfluidic platforms: advanced unit operations and applications. *Chem. Soc. Rev*, 44:6187, 2015. 6
- [22] A. E HERR, A. V HATCH, W. V GIANNOBILE, D. J THROCKMORTON, H. M TRAN, J. S BRENNAN, and A. K SINGH. Integrated Microfluidic Platform for Oral Diagnostics. *Annals of the New York Academy of Sciences*, 1098(1):362–374, mar 2007. 6
- [23] Roman Gerbers, Wilke Foellscher, Hong Chen, Constantine Anagnostopoulos, and Mohammad Faghri. From chip-in-a-lab to lab-on-a-chip: towards a single handheld electronic system for multiple application-specific lab-on-a-chip (ASLOC). 14:4042, 2014. 6
- [24] Kosuke Iwai, Ac Kuan, Cheng Shih, Xiao Lin, Thomas A Brubaker, Ryan D Sochol, Ac, and Liwei Lin. From chip-in-a-lab to lab-on-a-chip: towards a single handheld electronic system for multiple application-specific lab-on-a-chip (ASLOC). 14:3790, 2014. 6
- [25] Ka-Meng Lei, Pui-In Mak, Man-Kay Law, and Rui P. Martins. A NMR CMOS Transceiver Using a Butterfly-Coil Input for Integration With a Digital Microfluidic Device Inside a Portable Magnet. *IEEE Journal of Solid-State Circuits*, 51(10):2274–2286, oct 2016. 6
- [26] Quan Yuan, Kai Yang, and Jie Wu. Optimization of planar interdigitated microelectrode array for biofluid transport by AC electrothermal effect. *Microfluidics and Nanofluidics*, 16(1-2):167–178, jan 2014. 6
- [27] Ngoc M Pham, Sebastian Rusch, Yuksel Temiz, Robert D Lovchik, Hans-Peter Beck, Walter Karlen, and Emmanuel Delamarche. A bead-based immunogold-silver staining assay on capillary-driven microfluidics. 6

- [28] Benjamin Hannes, Julien Vieillard, Elie Bou Chakra, Radoslaw Mazurczyk, Colin D. Mansfield, Jan Potempa, Stanislas Krawczyk, and Michel Cabrera. The etching of glass patterned by microcontact printing with application to microfluidics and electrophoresis. *Sensors and Actuators B: Chemical*, 129(1):255–262, jan 2008. 6
- [29] Charles S. Henry, Min Zhong, Susan M. Lunte, Moon Kim, Haim Bau, and Jorge J. Santiago. Ceramic microchips for capillary electrophoresiselectrochemistry. *Analytical Communications*, 36(8):305–307, jan 1999. 6
- [30] Hamed Shadpour, Harrison Musyimi, Jifeng Chen, and Steven A Soper. Physiochemical properties of various polymer substrates and their effects on microchip electrophoresis performance. *Journal of Chromatography A*, 1111:238–251, 2006. 6
- [31] Andres W. Martinez, Scott T. Phillips, George M. Whitesides, and Emanuel Carrilho. Diagnostics for the Developing World: Microfluidic Paper-Based Analytical Devices. *Analytical Chemistry*, 82(1):3–10, jan 2010. 6
- [32] Christopher G. England, Emily B. Ehlerding, and Weibo Cai. NanoLuc: A Small Luciferase is Brightening up the Field of Bioluminescence. *Bioconjugate chemistry*, 27(5):1175, 2016. 8
- [33] Maïwenn Kersaudy-Kerhoas and Elodie Sollier. Micro-scale blood plasma separation: From acoustophoresis to egg-beaters. *Lab on a Chip*, 13(17):3323–3346, 2013. 10
- [34] Michael Reth. Matching cellular dimensions with molecular sizes. Technical report, 2013. 10
- [35] Richard W. Baker. *Membrane Technology and Applications*. John Wiley & Sons, Ltd, Chichester, UK, sep 2012. 11
- [36] Joon S. Shim, Andrew W. Browne, and Chong H. Ahn. An on-chip whole blood/plasma separator with bead-packed microchannel on COC polymer. *Biomedical Microdevices*, 12(5):949–957, 2010. 12
- [37] Veronica Betancur, Jianbo Sun, Nianqiang Wu, and Yuxin Liu. Integrated lateral flow device for flow control with blood separation and biosensing. *Micromachines*, 8(12), 2017. 12
- [38] Jun Ho Son, Sang Hun Lee, Soongweon Hong, Seung Min Park, Joseph Lee, Andrea M. Dickey, and Luke P. Lee. Hemolysis-free blood plasma separation. *Lab on a Chip*, 14(13):2287–2292, 2014. 12
- [39] Sara Thorslund, Oliver Klett, Fredrik Nikolajeff, Karin Markides, and Jonas Bergquist. A hybrid poly(dimethylsiloxane) microsystem for on-chip whole blood filtration optimized for steroid screening. *Biomedical Microdevices*, 8(1):73–79, mar 2006. 12
- [40] H. Walter and P.-Å. Albertsson. Fractionation of red blood cells by multiple sedimentation at unit gravity. *Experimental Cell Research*, 67(1):218–220, jul 1971. 13
- [41] Ivan K. Dimov, Lourdes Basabe-Desmots, Jose L. Garcia-Cordero, Benjamin M. Ross, Antonio J. Ricco, and Luke P. Lee. Stand-alone self-powered integrated microfluidic blood analysis system (SIMBAS). *Lab on a Chip*, 11(5):845–850, 2011. 13
- [42] Adam Samborski, Paweł Jankowski, Judyta Wgrzyn, Jacek A. Michalski, Sylwia Pawłowska, Sławomir Jakiela, and Piotr Garstecki. Blood diagnostics using sedimentation to extract plasma on a fully integrated point-of-care microfluidic system. *Engineering in Life Sciences*, 15(3):333–339, 2015. 13
- [43] Ju Nan Kuo and Yu Hui Zhan. Microfluidic chip for rapid and automatic extraction of plasma from whole human blood. *Microsystem Technologies*, 21(1):255–261, 2013. 14
- [44] Hojjat Madadi, Jasmina Casals-Terré, and Mahdi Mohammadi. Self-driven filter-based blood plasma separator microfluidic chip for point-of-care testing. *Biofabrication*, 7(2), 2015. 14

- [45] Andreas Lenshof, Asilah Ahmad-Tajudin, Kerstin Jarås, Ann-Margret Sward-Nilsson, Lena Åberg, Gyorgy Marko-Varga, Johan Malm, Hans Lilja, and Thomas Laurell. Acoustic Whole Blood Plasmapheresis Chip for Prostate Specific Antigen Microarray Diagnostics. *Analytical Chemistry*, 81(15):6030–6037, aug 2009. 14, 15
- [46] Kwang Hyo Chung, Yo Han Choi, Jong Heon Yang, Chan Woo Park, Wan Joong Kim, Chil Seong Ah, and Gun Yong Sung. Magnetically-actuated blood filter unit attachable to pre-made biochips. *Lab on a Chip*, 12(18):3272–3276, 2012. 15
- [47] Crispin Szydzik, Khashayar Khoshmanesh, Arnan Mitchell, and Christian Karnutsch. Microfluidic platform for separation and extraction of plasma from whole blood using dielectrophoresis. *Biomicrofluidics*, 9(6):1–16, 2015. 15
- [48] Stefan Haeberle, Thilo Brenner, Roland Zengerle, and Jens Duerée. Centrifugal extraction of plasma from whole blood on a rotating disk. 2006. 15, 16
- [49] Xiaoxi Yang, Omid Forouzan, Theodore P Brown, and Sergey S Shevkoplyas. Integrated separation of blood plasma from whole blood for microfluidic paper-based analytical devices. 16
- [50] Vivid. Vivid Plasma Separation Membrane - Diagnostics. 20
- [51] Martina Meinke, Gerhard Muller, Jurgen Helfmann, and Moritz Friebe. Optical properties of platelets and blood plasma and their influence on the optical behavior of whole blood in the visible to near infrared wavelength range. *Journal of Biomedical Optics*, 12(1):014024, 2007. 31
- [52] Meyer Burger Technology Ltd. PiXDRO LP50. 41
- [53] Harold P. Erickson. Size and Shape of Protein Molecules at the Nanometer Level Determined by Sedimentation, Gel Filtration, and Electron Microscopy. *Biological Procedures Online*, 11(1):32–51, dec 2009. 54

# Appendix A

## Milling details

For fabrication of the devices a Roland MDX-40A micromilling machine is used. Using the program SRP Player, the machine can be programmed. Table A.1 shows the parameters that need to be set in the machine to obtain the desired results. The milling time for completing one whole device is 30 minutes. A faster cutting time can be obtained by increasing the feed rate in the finishing step. However, this increases the risk of breaking the 0.5 mm drill bit.

Table A.1: Milling parameters

<b>parameter</b>	<b>step 1: roughing</b>	<b>step 2: finishing</b>
flat [mm]	1	0.5
feed rate [mm/min]	360	100
spindle [rpm]	10000	10000
cutting-in amount [mm]	0.07	0.10
path interval [mm]	0.60	0.10
finish margin [mm]	0.05	0.00

## Appendix B

### Pluronic F-127 durability

The hydrophilic Pluronic F-127 coating was tested on durability over time in different storage conditions. A piece of PMMA was submerged in 10 w/v% Pluronic F-127 in MilliQ water for 24h. Then the different pieces were stored at different conditions: in air, in water, in the dark and in air, in the dark and in water and in the dark in vacuum. Since there was no set-up available for storage in vacuum a piece of aluminium foil was wrapped around the PMMA and air was sucked out with a vacuum pump to minimise the amount of air. Table B.1 shows the results of contact angle measurement after 2 weeks.

Table B.1: Contact angle of water on PMMA coated with Pluronic F-127 after 2 weeks in different storage conditions

storage conditions	contact angle [°]
air	39.58
water	63.13
dark and air	59.17
dark and water	65.09
dark and vacuum	23.76

# Appendix C

## Inkjet printing

For the application of the LUMABS sensor it was explored to use inkjet printing. Unfortunately, the preliminary results were not promising and therefore it was chosen to use pipetting to apply the LUMABS sensor onto the chip. This appendix explains the steps that were taken in the process. The Pixdro LP50 inkjet printer was used in combination with 10 pL cartridges from Fujifilm with a nozzle opening of  $21.5 \mu\text{m}$  [52].

The first step was to develop inks containing the LUMABS sensor that had the correct physical properties for inkjet printing and were also a good environment for the LUMABS sensor. The inks were based on phosphate-buffered saline (PBS) in combination with glycerol to facilitate stable drying of the sensor. Furthermore, Tween-20 is added to lower the surface tension. Three different inks were made with glycerol concentrations of 10%, 25% and 50%. The density of these inks was measured at  $20^\circ\text{C}$  with a DMA 1001 density meter from Anton Paar. The surface tension was measured with a dataphysics OCA-30 measurement set-up. Finally, the viscosity was measured at  $25^\circ\text{C}$  with a MARS 60 rheometer from Thermofisher scientific. Table C.1 shows the measured properties of the inks.

Table C.1: Density of the different inks.

ink no.	glycerol [%]	density [ $\text{kg}/\text{m}^3$ ]	surface tension [ $\text{mN}/\text{m}$ ]	dynamic viscosity [ $\text{Pa}\cdot\text{s}$ ]
1	10	1035.51	46.466	0.0011805
2	25	1083.56	46.33	0.0021055
3	50	1144.29	50.51	0.006984

It was chosen to proceed with ink 3 with a glycerol percentage of 50. The higher glycerol percentage could potentially help the preservation of the LUMABS and the viscosity is closest to the desired viscosity. In order to lower the surface tension, more Tween-20 could be added.

Since the Pixdro LP50 uses piezoelectric elements to create droplets, a waveform needed to be developed. For this project a waveform is used that ramps to a voltage of 50 V in  $5 \mu\text{s}$ , then stays at 50 V for  $30 \mu\text{s}$  then the voltage is decreased to 0 V again in  $10 \mu\text{s}$ . Furthermore, an ink-pressure of 0.7 mbar is used.

Unfortunately, the results from the inkjet printing were very inconsistent and it was hard to control the amount of sensor added into the chambers. Since the results from pipetting were good it was decided to not continue with the optimisation of the inkjet printing. An extensive literature study on inkjet printing and a practical study into the effects of the properties of the inks and the different waveforms need to be done in order to determine the potential of inkjet printing in this particular application.



## Appendix D

# Blood collection by fingerprick

A procedure was set up to facilitate blood collection by a fingerprick from voluntary participants. On the following two pages, a procedure and an informed consent can be found. These two documents should be handed to the donor before donation. The donor should prick him/herself and collect the blood in a capillary tube. This capillary tube can then be emptied on the POCT device. It is important that the donation is done in a calm and clean area and that the consumables (capillary tube, wipes etc.) are disposed in a biohazard container. Furthermore, the lancet should be disposed of in a special container for biohazard sharps.

1. Wash your hands with water and soap. Make sure to rinse and dry well.
2. Use a disinfection swab to disinfect the finger you want to puncture. Wait for the disinfectant to evaporate.
3. Take a single use lancet and remove the sterile cover. Do not use when this cover is already removed.
4. Take the lancet between your index and middle finger of your dominant hand.
5. Place the lancet tip at the side of the finger you want to prick from. Preferably this the ring finger of your not dominant hand. The best place to prick is shown in this image:



6. Press the lancet on your skin and push the button. The lancet will shortly puncture your finger.
7. Use a sterile tissue to remove the first drop of blood.
8. Take the capillary tube and place it against the puncture. The tube will fill with blood. It is advisable to hold your punctured finger upside down. Pressure can be applied slightly to your finger, but do not try to 'milk' your finger as this is not beneficial for the blood quality.

<b>Informed consent</b>	Author: Emma Moonen	<b>TU/e</b>
	Version: 1.0	
	Date: 10/07/2019	

You are being asked to donate blood by means of a finger prick for research purposes. This research aims to develop a Point-of-care testing chip for faster and easier detection of therapeutic drugs in the blood. Your blood will only be used to test the fluid flow of whole blood through the system and no biological/pathological measurements will be performed with your blood.

During this donation you will perform a finger prick on yourself. You will be given enough information and support on how to do this. After the finger prick the blood (100 microliter) will be collected in a capillary tube. This capillary tube will then be emptied on the microfluidic chip.

All materials used in this experiment are single use and will be disposed of after usage. No personal data is collected, and the blood will not be stored.

By continuing with the donation of blood I give my consent that I:

1. Voluntarily want to participate in this research
2. Have gotten information about the research and I understood this information
3. Read the procedure and understand it.
4. Know I am free to stop the donation whenever I want

# Appendix E

## Plasma extraction

Multiple design iterations are done towards the final plasma extraction structure. In this appendix the tested capillary pumps are showed and the changes are explained.

Figures E.1, E.2 and E.3 show the first capillary pump design that were made using micromilling. Since the smallest drill bit that can be used in the micromilling machine is 500  $\mu\text{m}$  in diameter, the smallest channel in the design can not be smaller than 500  $\mu\text{m}$ .

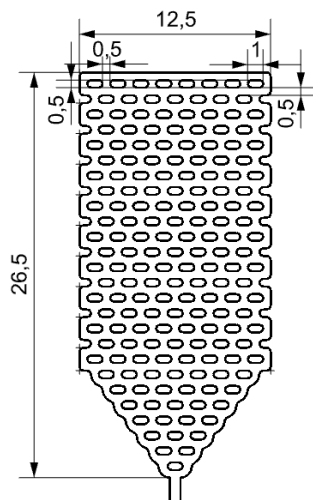


Figure E.1: Capillary pump design with multiple rows and columns of pillars. Channel width and depth 500  $\mu\text{m}$  pillar dimension 500x1000  $\mu\text{m}$ . Dimensions in figure in millimetres.

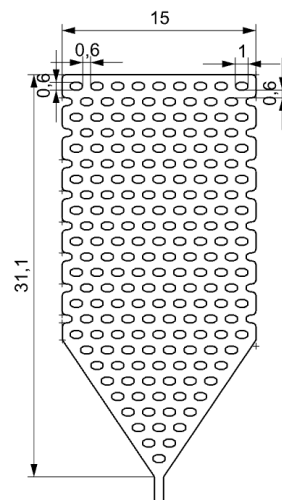


Figure E.2: Capillary pump design with multiple rows and columns of pillars. Channel width and depth 600  $\mu\text{m}$  pillar dimension 600x1000  $\mu\text{m}$ . Dimensions in figure in millimetres.

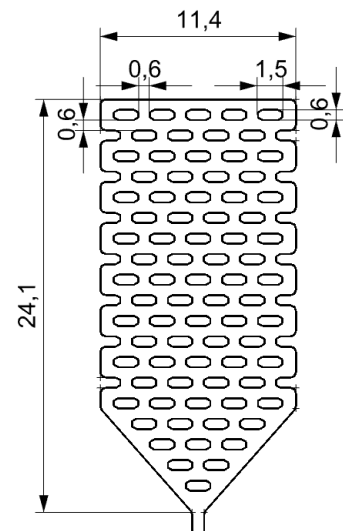


Figure E.3: Capillary pump design with multiple rows and columns of pillars. Channel width and depth 600  $\mu\text{m}$  pillar dimension 600x1500  $\mu\text{m}$ . Dimensions in figure in millimetres.

It was observed that the volume of the designed capillary pumps was too large. The maximum blood sample volume from a fingerprick is around 100  $\mu\text{L}$ . If plasma extraction would be optimised around 55  $\mu\text{L}$  of plasma could be obtained from 100  $\mu\text{L}$  of whole blood, Therefore, the total system volume should not be larger than approximately 50  $\mu\text{L}$ . Therefore, new designs with a maximum volume of 30  $\mu\text{L}$  were made and tested. These designs can be found in Figures E.4, E.5 and E.6.

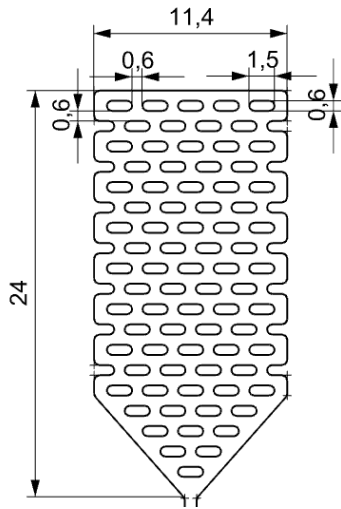


Figure E.4: Capillary pump design with multiple rows and columns of pillars. Channel width and depth 600  $\mu\text{m}$  pillar dimension 600x1500  $\mu\text{m}$ . Dimensions in figure in millimetres.

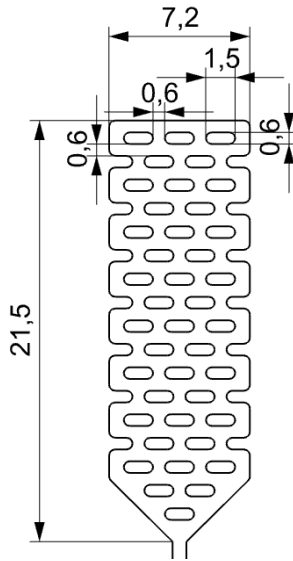


Figure E.5: Capillary pump design with multiple rows and columns of pillars. Channel width and depth 600  $\mu\text{m}$  pillar dimension 600x1500  $\mu\text{m}$ . Dimensions in figure in millimetres.

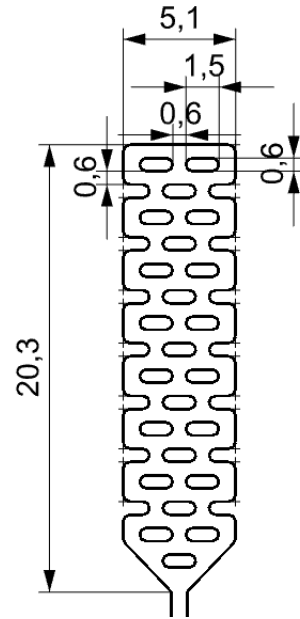


Figure E.6: Capillary pump design with multiple rows and columns of pillars. Channel width and depth 600  $\mu\text{m}$  pillar dimension 600x1500  $\mu\text{m}$ . Dimensions in figure in millimetres.

It was observed that the volume of the designed capillary pumps was still to large. Therefore, new capillary pumps were designed with a smaller volume. Furthermore, designs were made with features smaller than 500  $\mu\text{m}$  which were 3D printed with an Objet 30 Polyjet printer. Figures E.7 to E.15 were all designed, fabricated and tested. Unfortunately none of the structures were able to extract plasma from whole blood. Furthermore, the 3D printer was not able to print the pumps in Figure E.7, E.8 and E.9. The channels were not open since 3D print material was molten into the channels.

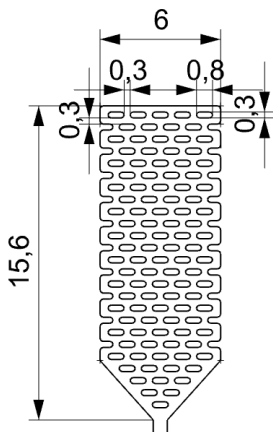


Figure E.7: Capillary pump design with multiple rows and columns of pillars. Channel width and depth 300  $\mu\text{m}$  pillar dimension 300x800  $\mu\text{m}$ . Dimensions in figure in millimetres.

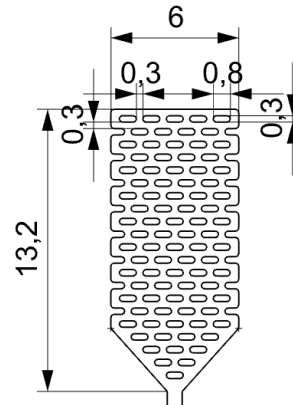


Figure E.8: Capillary pump design with multiple rows and columns of pillars. Channel width and depth 300  $\mu\text{m}$  pillar dimension 300x800  $\mu\text{m}$ . Dimensions in figure in millimetres.

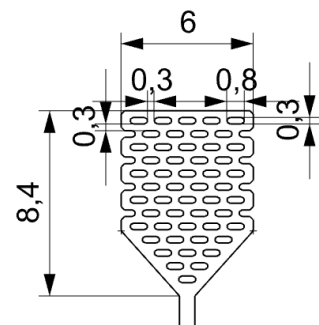


Figure E.9: Capillary pump design with multiple rows and columns of pillars. Channel width and depth 300  $\mu\text{m}$  pillar dimension 300x800  $\mu\text{m}$ . Dimensions in figure in millimetres.

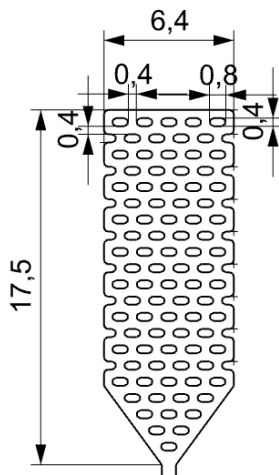


Figure E.10: Capillary pump design with multiple rows and columns of pillars. Channel width and depth  $400\ \mu\text{m}$  pillar dimension  $400\times 800\ \mu\text{m}$ . Dimensions in figure in millimetres.

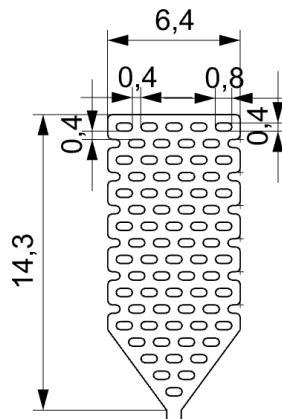


Figure E.11: Capillary pump design with multiple rows and columns of pillars. Channel width and depth  $400\ \mu\text{m}$  pillar dimension  $400\times 800\ \mu\text{m}$ . Dimensions in figure in millimetres.

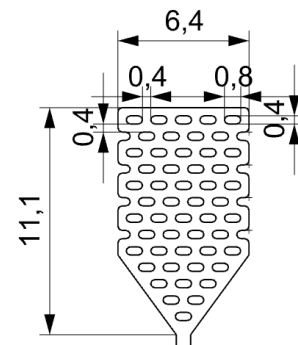


Figure E.12: Capillary pump design with multiple rows and columns of pillars. Channel width and depth  $400\ \mu\text{m}$  pillar dimension  $400\times 800\ \mu\text{m}$ . Dimensions in figure in millimetres.

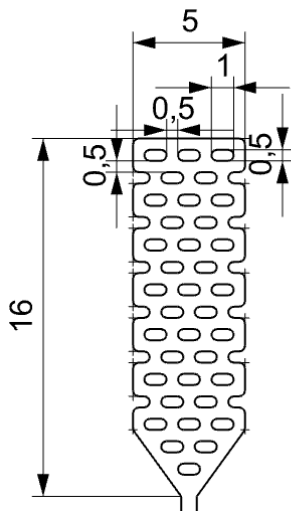


Figure E.13: Capillary pump design with multiple rows and columns of pillars. Channel width and depth  $500\ \mu\text{m}$  pillar dimension  $500\times 1000\ \mu\text{m}$ . Dimensions in figure in millimetres.

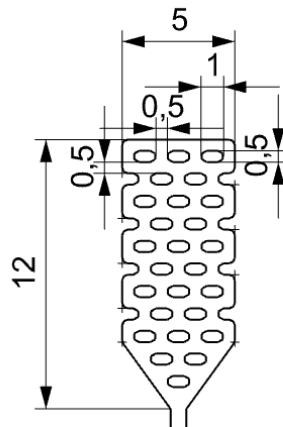


Figure E.14: Capillary pump design with multiple rows and columns of pillars. Channel width and depth  $500\ \mu\text{m}$  pillar dimension  $500\times 1000\ \mu\text{m}$ . Dimensions in figure in millimetres.

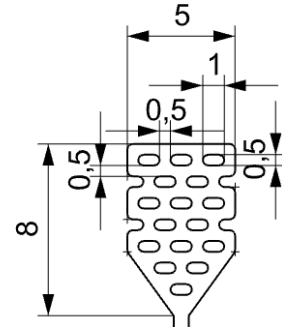


Figure E.15: Capillary pump design with multiple rows and columns of pillars. Channel width and depth  $500\ \mu\text{m}$  pillar dimension  $500\times 1000\ \mu\text{m}$ . Dimensions in figure in millimetres.

The final capillary pumps structures are shown in Figure E.17 and E.16. Both these capillary pumps work and create enough capillary action to wick the plasma from the plasma extraction membrane. Since the volume of the shorter capillary pump is smaller, this design was chosen as final design.

Although the designs do not seem to be very different from each other, only the capillary pumps in Figures E.16 and E.17 were able to facilitate plasma extraction. This is also because the filter surface area was varied and the sealing was optimised.

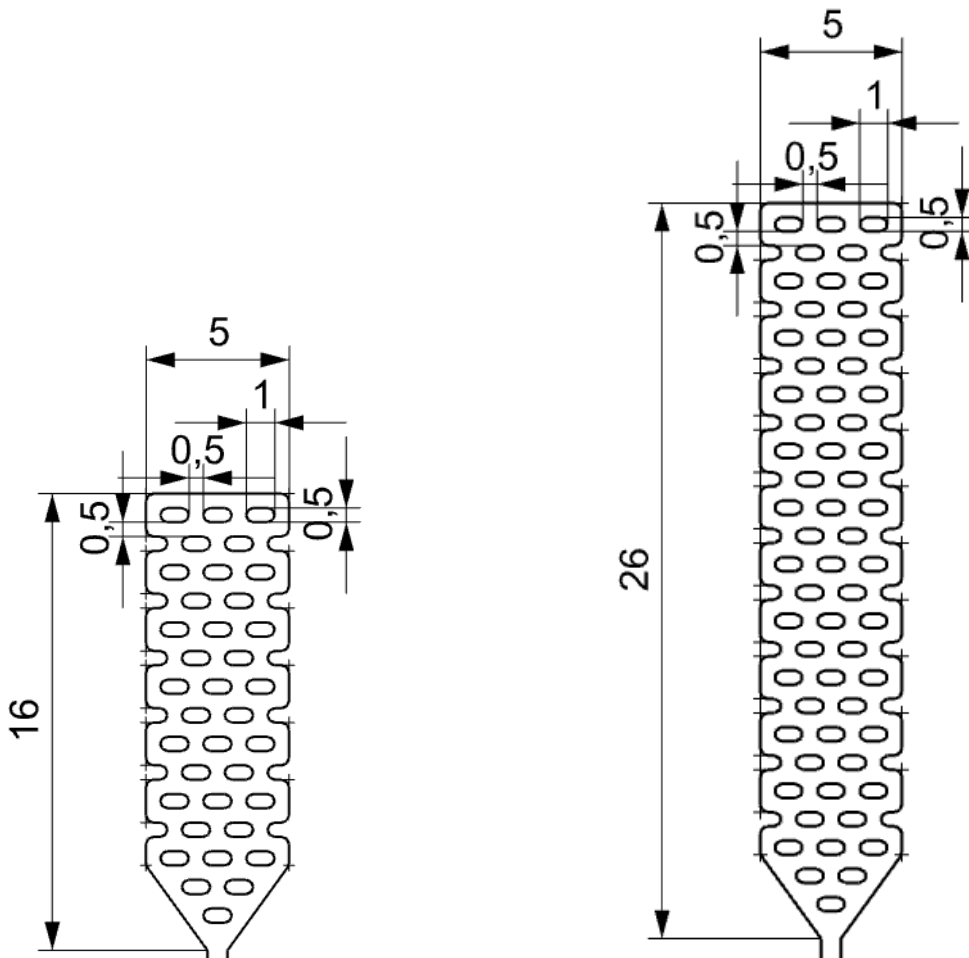


Figure E.16: Capillary pump design with multiple rows and columns of pillars. Channel width and depth 500  $\mu\text{m}$  pillar dimension 500x1000  $\mu\text{m}$ . Dimensions in figure in millimetres.

Figure E.17: Capillary pump design with multiple rows and columns of pillars. Channel width and depth 500  $\mu\text{m}$  pillar dimension 500x1000  $\mu\text{m}$ . Dimensions in figure in millimetres.

# Appendix F

## Appendix Matlab

```
1 % Written by Emma Moonen
2 % 2019
3 % Read thesis/manual for more information on how to use
4
5 clear all; close all;
6
7 %% Define variables here
8
9 %Define directory and folder of photos to analyse
10 directory = 'C:\Users\s146776\Documents\Afstudeerproject\meetresultaten TUE
    \Luminescence\13_08_2019\';
11 folder = '17. 199 fmol white pluronic';
12
13 %Define start and stop photo/minute
14 start = 0;
15 stop = 21;
16
17 %Define luminescence threshold
18 thresholdValueLow = 14;
19 thresholdValueHigh = 16;
20
21 %% Reading and formatting of image
22
23 path = strcat(directory, folder);
24 addpath(path)
25
26 no_images = length(dir(folder))-2;
27 file_name=dir(strcat(folder));
28
29 for n=3:no_images+2
30     image_{n-2}=imread(file_name(n).name);
31 end
32
33 no_images = stop-start;
34
35 for n=1:(stop-start)
```



```

36     image_{n}=image_{start+n};
37 end
38
39 for n=1:no_images
40     image_{n} = imcrop(image_{n},[2000,1000,2000,2000]);
41 end
42
43 warning('off', 'Images:initSize:adjustingMag');
44
45 imshow(image_{1})
46
47 w = 140;
48 h = 110;
49 message = sprintf('Click the upper left corner of the cropping box');
50 uiwait(msgbox(message));
51 [x, y] = ginput(1); % Ask user to click the upper left corner.
52
53 for n=1:no_images
54     image_{n} = imcrop(image_{n},[x,y,w,h]);
55 end
56
57
58 %% Convert images to grayscale and binary according to luminescence
59     threshold values
60 size_image = size(image_{1});
61 for n=1:no_images
62     image_gray_{n} = rgb2gray(image_{n});
63     for i=1:size_image(1)
64         for j=1:size_image(2)
65             if image_gray_{n}(i,j) < thresholdValueHigh && image_gray_{n}(i
66                 ,j) > thresholdValueLow
67                 image_binary_{n}(i,j) = 1;
68             else
69                 image_binary_{n}(i,j) = 0;
70             end
71         end
72     end
73     image_binary_{n} = imfill(image_binary_{n}, 'holes');
74 end
75 % Turn these lines on if you want to display the photos and the binary
76 % equivalent
77 figure(2)
78 i=1;
79 for n=1:no_images
80     subplot(no_images,2,i)
81     imshow(image_{n})
82     i=i+1;
83     subplot(no_images,2,i)
84     imshow(image_binary_{n})

```

```

85     i=i+1;
86 end
87
88 %% Processing of RGB/HSV data
89
90 for n=1:no_images
91     R_{n} = image_{n}(:, :, 1);
92     G_{n} = image_{n}(:, :, 2);
93     B_{n} = image_{n}(:, :, 3);
94 end
95
96 for n=1:no_images
97     hsvValues_{n} = rgb2hsv(image_{n});
98     hueValue_{n} = hsvValues_{n}(:, :, 1);
99     satValue_{n} = hsvValues_{n}(:, :, 2);
100    valValue_{n} = hsvValues_{n}(:, :, 3);
101 end
102
103 %Find indices equal to 1 in binary image
104 for n=1:no_images
105     indices_x = [];
106     indices_y = [];
107     for i=1:size_image(1)
108         for j=1:size_image(2)
109             if image_binary_{n}(i,j) == 1
110                 indices_x = [indices_x , i];
111                 indices_y = [indices_y , j];
112             end
113         end
114     end
115     indices_x_{n} = indices_x;
116     indices_y_{n} = indices_y;
117 end
118
119 %Retrieve GB and hue data for the pixels in the luminescence threshold area
120 for n=1:no_images
121     for i=1:length(indices_x_{n})
122         x = indices_x_{n}(i);
123         y = indices_y_{n}(i);
124         G_new_{n}(i) = G_{n}(x,y);
125         B_new_{n}(i) = B_{n}(x,y);
126         hueValue_new_{n}(i) = hueValue_{n}(x,y);
127         satValue_new_{n}(i) = satValue_{n}(x,y);
128         valValue_new_{n}(i) = valValue_{n}(x,y);
129     end
130 end
131
132 hueValue_ = hueValue_new_;
133 satValue_ = satValue_new_;
134 valValue_ = valValue_new_;
135

```

```
136 for n=1:no_images
137     G_new_{n} = double(G_new_{n});
138     B_new_{n} = double(B_new_{n});
139 end
140
141
142 %% Calculating the g/b ratios
143
144 for n=1:no_images
145     green_blue_ratio= cellfun(@(x,y) x/y, G_new_,B_new_, 'un',0);
146     green_blue_ratio_avg = cellfun(@mean2, green_blue_ratio, 'un',0);
147     g = cellfun(@mean2, G_new_, 'un',0);
148     b = cellfun(@mean2, B_new_, 'un',0);
149 end
150
151 g = cell2mat(g);
152 b = cell2mat(b);
153 mean_g = mean(g);
154 std_g = std(g);
155 mean_b = mean(b);
156 std_b = std(b);
157
158 green_blue_ratio = cell2mat(green_blue_ratio);
159 mean_gb_ratio = mean(green_blue_ratio);
160 std_gb_ratio = std(green_blue_ratio);
161
162 %% Calculating the hue value
163
164 for n=1:no_images
165     average_hue = cellfun(@mean2, hueValue_ , 'un',0);
166     average_sat = cellfun(@mean2, satValue_ , 'un',0);
167     average_val = cellfun(@mean2, valValue_ , 'un',0);
168 end
169
170 average_hue = cell2mat(average_hue);
171 average_sat = cell2mat(average_sat);
172 average_val = cell2mat(average_val);
173 mean_hue = mean(average_hue) * 360;
174 mean_sat = mean(average_sat);
175 mean_val = mean(average_val);
176 std_hue = std(average_hue);
177
178 %% Printing the values
179 fprintf('mean gb/ratio: %f \n',mean_gb_ratio)
180 fprintf('std gb/ratio: %f \n', std_gb_ratio)
181 fprintf('mean g : %f \n', mean_g)
182 fprintf('mean b : %f \n', mean_b)
183
184 %% Plotting
185
186 figure(1)
```

```
187 time = [start:stop-1];  
188 plot(time, green_blue_ratio, 'o')  
189 title('g/b ratio over time')  
190 xlabel('time [minutes]')  
191 ylabel('g/b ratio [-]')
```

## Appendix G

# Diffusion in the chip

Since diffusion is a complex mechanism, several assumptions need to be made in order to estimate the diffusion in the chip. The diffusion of the LUMABS molecule is modelled as a single sphere diffusing along a single dimension. Based on the weight of the LUMABS of 72 kDa, the minimum size of a sphere were this weight fits in can be calculated [53]:

$$r_{min} = 0.066 \cdot M^{1/3} = 0.066 \cdot (72 \cdot 10^3)^{1/3} = 2.746\text{nm} \quad (\text{G.1})$$

The self diffusion coefficient for isolated spheres is given by the Stokes-Einstein equation:

$$D = \frac{k_b T}{6\pi\eta r} \quad (\text{G.2})$$

With  $k_b$  the Boltzmann constant ( $1.380649 \cdot 10^{-23}$  J/K),  $T$  the absolute temperature,  $\eta$  the viscosity of the suspending fluid and  $r$  the radius of the sphere as defined in Equation G.1.

A characteristic time  $\tau$  for the diffusion of a molecule over the characteristic length  $h$  can then be defined as:

$$\tau = \frac{h^2}{6D} \quad (\text{G.3})$$

When taking  $h = 8$  mm, from the centre of the detection chamber to the centre of the substrate chamber and  $D = 74 \mu\text{m}^2/\text{s}$ , the diffusion time is equal to 2402 minutes or 40 hours.

## **Appendix H**

# **TU/e code of scientific conduct**

## Declaration concerning the TU/e Code of Scientific Conduct for the Master's thesis

I have read the TU/e Code of Scientific Conduct<sup>i</sup>.

I hereby declare that my Master's thesis has been carried out in accordance with the rules of the TU/e Code of Scientific Conduct

Date

25-09-2019

Name

Emma Moonen

ID-number

0895596

Signature



*Submit the signed declaration to the student administration of your department.*

<sup>i</sup> See: <http://www.tue.nl/en/university/about-the-university/integrity/scientific-integrity/>

The Netherlands Code of Conduct for Academic Practice of the VSNU can be found here also.  
More information about scientific integrity is published on the websites of TU/e and VSNU